ADVANCING EARTH AND SPACE SCIENCES

Geochemistry, Geophysics, Geosystems

RESEARCH ARTICLE
10.1029/2024GC012069

Special Collection:
Through the Arctic Lens: Progress in Understanding the Arctic Ocean, Margins and Landmasses

Key Points:

- A non-thermal effect on brGDGT paleotemperature estimates in lakes is identified by the isomer ratio IR_{6Me}
- The calibration of MBT'_{5Me} to temperature in middle and high latitude lakes is strengthened if samples with $IR_{6Me} > 0.4$ are excluded
- IR_{6Me} does not appear to identify non-thermal effects on tropical lake samples, but this could change as the data set is expanded

Supporting Information:

Supporting Information may be found in the online version of this article.

Correspondence to:

J. B. Novak,
jobnovak@ucsc.edu

Citation:

Novak, J. B., Russell, J. M., Lindemuth, E. R., Prokopenko, A. A., Pérez-Angel, L., Zhao, B., et al. (2025). The branched GDGT isomer ratio refines lacustrine paleotemperature estimates. *Geochemistry, Geophysics, Geosystems*, *26*, e2024GC012069. https://doi.org/10.1029/2024GC012069

Received 22 NOV 2024
Accepted 15 FEB 2025

Author Contributions:

Conceptualization: Joseph B. Novak, Pratigya J. Polissar
Data curation: Joseph B. Novak, Boyang Zhao, George E. A. Swann
Formal analysis: Boyang Zhao, George E. A. Swann, Pratigya J. Polissar

The Branched GDGT Isomer Ratio Refines Lacustrine Paleotemperature Estimates

Joseph B. Novak[1], James M. Russell[2], Emma R. Lindemuth[1], Alexander A. Prokopenko[3], Lina Pérez-Angel[2], Boyang Zhao[2], George E. A. Swann[4], and Pratigya J. Polissar[1]

[1]Ocean Sciences, University of California, Santa Cruz, CA, USA, [2]Department of Earth, Environmental, and Planetary Sciences, Brown University, Providence, RI, USA, [3]Insititue of Mineralogy, University of Cologne, Cologne, Germany, [4]School of Geography, University of Nottingham, Nottingham, UK

Abstract Branched glycerol dialkyl glycerol tetraethers (brGDGTs) are membrane-spanning lipids synthesized by bacteria in numerous substrates. The degree of methylation of the five methyl brGDGTs in both soils and lake sediments, described by the MBT'_{5Me} index, is empirically related to surface atmospheric temperature. This relationship in lakes is generally assumed to reflect lake surface temperatures captured by brGDGT production in the water column and exported to lake sediments, and the MBT'_{5Me} index has been applied to brGDGTs in lake sediment successions to reconstruct changes in temperature through time. We analyzed the relationship between MBT'_{5Me} and the isomerization of brGDGTs (IR_{6Me}) in globally distributed surficial lake sediments and demonstrated that the relationship, and calibrations, of MBT'_{5Me} and temperature in middle and high latitude lakes are sensitive to incompletely understood factors related to IR_{6Me}. IR_{6Me} does not appear to track a non-thermal influence of brGDGT methylation in tropical lakes, but this could change as the data set is expanded. We address ongoing challenges in the application of the MBT'_{5Me} paleothermometer in middle and high latitude lakes with new MBT'_{5Me}-temperature calibrations based on grouping lakes by IR_{6Me}. We demonstrate how IR_{6Me} can distinguish samples with a significant non-thermal influence on MBT'_{5Me} by targeting anomalously warm temperatures during the Last Glacial Maximum from newly analyzed piston and gravity core samples from Lake Baikal, Russia.

Plain Language Summary Branched glycerol dialkyl glycerol tetraethers are fats used by bacteria to build their cell walls. Bacteria build their cell walls with different kinds of brGDGTs in response to ambient temperature. BrGDGTs are often preserved in lake sediments, making them a useful tool for reconstructing past climate. While working on samples from Lake Baikal, Russia, we noticed unexpectedly warm temperatures during the last ice age estimated from brGDGTs. These warm temperatures coincided with unusually high relative amounts of 6-methyl brGDGTs. This observation spurred the analysis of a large data set of published globally distributed lake brGDGT data. We found that samples from middle and high latitude lakes with relatively more 6-methyl brGDGTs tended to have higher than expected brGDGT-estimated temperatures. We use our findings to refine the equations that relate brGDGT distributions to surface air temperature in middle and high latitude lake sediments.

1. Introduction

Paleoclimate data are the only means of testing the performance of models used to simulate Earth's climate under boundary conditions drastically different from those used today (Braconnot et al., 2012). Temperature is an essential parameter for such comparisons, capturing the local and global energy balance (Tierney et al., 2020). Although several methods exist for quantifying past sea surface temperatures, reconstructing terrestrial paleotemperatures has proven more difficult. Fossil branched glycerol dialkyl glycerol tetraethers (brGDGTs), membrane spanning lipids produced by some bacteria (Chen et al., 2022; Halamka et al., 2023), hold great promise as a paleotemperature proxy biomarker because of their apparently ubiquitous response to temperature across numerous growth media (Raberg, Miller, et al., 2022). Yet challenges remain in their widespread application due to temperature estimates observed for past soils and sediments that sometimes disagree strongly with other paleoclimate data (Acharya et al., 2023; Cluett et al., 2023; Inglis et al., 2019; Kielhofer et al., 2023; Zhu et al., 2021).

Structurally, brGDGTs are characterized by straight alkyl core chains with zero to two cyclopentyl moieties and four to six methyl groups (Damsté et al., 2000; De Jonge et al., 2014; Weijers et al., 2007). The methylation of

Funding acquisition: Joseph B. Novak, Pratigya J. Polissar
Investigation: Joseph B. Novak, Emma R. Lindemuth, Pratigya J. Polissar
Methodology: Joseph B. Novak, James M. Russell
Project administration: Pratigya J. Polissar
Resources: James M. Russell, George E. A. Swann, Pratigya J. Polissar
Supervision: Pratigya J. Polissar
Visualization: Joseph B. Novak
Writing – original draft: Joseph B. Novak
Writing – review & editing: Joseph B. Novak, James M. Russell, Emma R. Lindemuth, Boyang Zhao, George E. A. Swann, Pratigya J. Polissar

brGDGTs is thought to be altered by bacteria in response to temperature to maintain cell membrane fluidity and permeability (Naafs et al., 2021; Weijers et al., 2007; Zhang & Rock, 2008). There have been extensive calibration efforts to relate the methylation of brGDGTs to temperature in lakes, peats, and soils (De Jonge et al., 2014; Dearing Crampton-Flood et al., 2020; Martínez-Sosa et al., 2021; Naafs, Inglis, et al., 2017; Peterse et al., 2012; Raberg, Miller, et al., 2022; Raberg et al., 2021; Russell et al., 2018; Zhao et al., 2021, 2023). Analyses of the relationship of MBT'_{5Me} to temperature in tropical lakes have produced statistically strong calibrations (e.g., Russell et al., 2018; Zhao et al., 2023). However, the calibration of brGDGT methylation in extratropical lakes to temperature has yielded weaker relationships with much higher uncertainty than in tropical lakes (Cao et al., 2020; Martínez-Sosa et al., 2021; Raberg et al., 2021; Zhao et al., 2023). The sources of this uncertainty remain unclear and limit the utility of brGDGT paleotemperature estimates in these regions.

Analytical developments have improved brGDGT calibrations but have not resolved the issues in middle and high latitude regions. The first generation of brGDGT analyses (Hopmans et al., 2000; Weijers et al., 2007) was unable to separate the five and six methyl brGDGT isomers. Subsequently, improved methods separated these isomers (De Jonge et al., 2014; Hopmans et al., 2016), leading to the development of the MBT'_{5Me} index, which describes the relative abundance of temperature-sensitive 5-methyl brGDGTs (De Jonge et al., 2014). Later work linked the distribution of 6-methyl brGDGTs, characterized by the isomer ratio of 5- to 6-methyl brGDGTs (IR_{6Me}), and the associated non-thermal influence on MBT'_{5Me} with lake water salinity (Kou et al., 2022; Wang et al., 2021), dissolved oxygen (Wu et al., 2021), and pH (Raberg, Miller, et al., 2022). A subsequent study of Central European lakes showed a deviation from the expected temperature-MBT'_{5Me} relationship in sediment samples where IR_{6Me} was greater than 0.5 (i.e., when 6-methyl brGDGTs were more abundant than 5-methyl) (Bauersachs et al., 2024), similar to earlier findings in a study of global soils (Naafs, Inglis, et al., 2017). Others attempted to deconvolve the non-thermal influence on MBT'_{5Me} from tetramethylated brGDGTs thought to be produced in association with the 6-methyl brGDGT isomer set rather than the 5-methyl brGDGT isomer set alone via a two-endmember mixing model (Wang et al., 2024). These studies highlight the behavior of the MBT'_{5Me} -temperature relationship with changing IR_{6Me} but do not clarify why brGDGT isomerization is associated with aberrant temperature estimates in some samples or provide a robust mechanism to identify samples that may have non-thermal influences.

Here, we analyze brGDGT distributions in a compilation of global lacustrine surface sediment data to test whether IR_{6Me} can improve the MBT'_{5ME} temperature calibration by excluding samples with non-thermal influences. We then demonstrate that IR_{6Me} distinguishes between different populations of brGDGTs in new analyses of archived samples from Lake Baikal, Russia, and present an approach to estimating paleotemperatures in MBT'_{5Me} timeseries with an apparent non-thermal influence.

2. Materials and Methods

2.1. Lake Baikal Geologic Setting, Materials, Composite Section, and Age Determination

Lake Baikal, Russia (53°30′N, 108°0′E), is a rift lake in southern Siberia that formed approximately 30 million years ago within the Baikal rift zone (Petit & Déverchère, 2006). Today, the climate in the Lake Baikal region is characterized by high continentality (Colman et al., 1995) with an average annual air temperature range of ~40°C, with maximum air temperature (15–20°C) in July and minimum air temperature (−20 to −25°C) in January according to ERA-40 reanalysis data (Kouraev et al., 2007). Surface water temperatures reach a maximum 10–12°C in August and a minimum in January, when lake surface waters freeze (Hampton et al., 2008). Ice cover typically persists for 4–6.5 months, depending on a given year's climate conditions and which region of the lake (north vs. south basin) is considered (Kouraev et al., 2007).

We measured brGDGTs in 77 subsamples that cover the past 250 thousand years from cores 333-PC2, 340-TC1, 340-PC1, VER92/2-GC24 and 12 surficial samples from several multicores and box cores (Carter & Colman, 1994; E. Karabanov et al., 2004; Peck et al., 1994; Roberts et al., 2018; Swann et al., 2018) (Figure 1a). Dry bulk density (DBD) from cores 333-PC2, 340-TC1, and 340-PC1 was correlated to generate a continuous composite section (Figure S1 in Supporting Information S1) since these cores are all from the Academician Ridge region of the lake (Figure 1). DBD changes are large and primarily a function of the glacial-interglacial variations in diatomaceous ooze and clay content in the Lake Baikal cores, which vary on glacial-interglacial timescales (Peck et al., 1994). Magnetic susceptibility profiles (Peck et al., 1994) of cores 333-PC2, 340-TC1, and 340-PC1 placed in our composite section are in good agreement (Figure S2 in Supporting Information S1), indicating that our correlation of the cores' physical properties is robust. Our 333–340 composite section was then assigned age

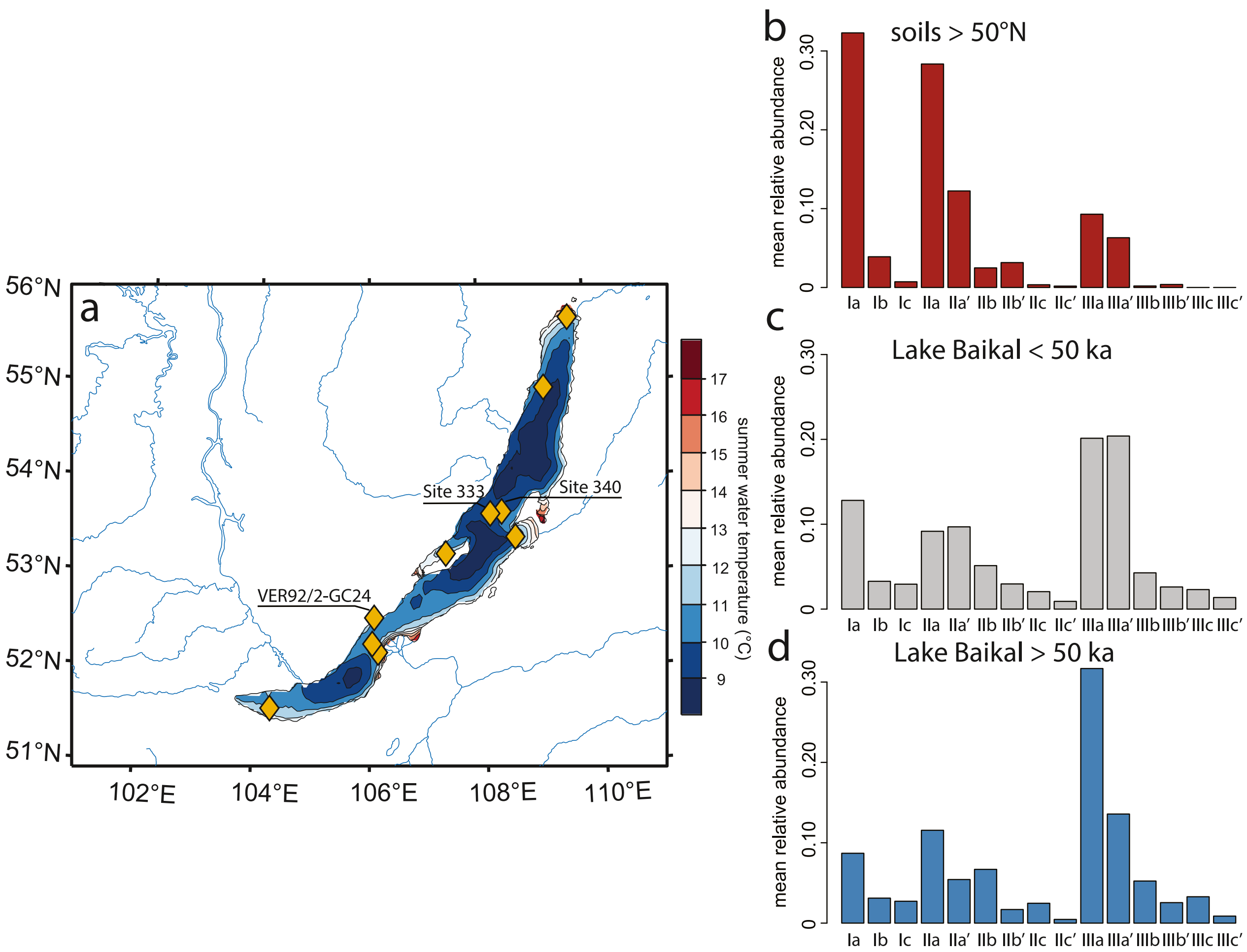

Figure 1. Distribution of brGDGTs in Lake Baikal sediments. (a) Map of Lake Baikal showing core locations. Contours show mean summer water temperatures reported by Carrea and Merchant (2019). (b) Mean relative abundances of individual brGDGTs in soils >50°N (Dearing Crampton-Flood et al., 2020). (c) Mean relative abundances of individual brGDGTs in Lake Baikal sediments from the last 50 Ka. (d) Mean relative abundances of brGDGTs in Lake Baikal sediments from the 50 to 250 Ka interval.

by correlating dry bulk density to the orbitally tuned BDP-96 biogenic silica record (Prokopenko et al., 2006), supplemented by published radiocarbon dates (Peck et al., 1994) and an assumed core top age of 0 Ka (Figure S3 in Supporting Information S1). Core VER92/2-GC24 was assigned age from a highly resolved series of ^{14}C ages (E. Karabanov et al., 2004). Surficial sample ages are assumed to be late Holocene, which is supported by ^{210}Pb chronologies on adjacent multicores (Roberts et al., 2018; Swann et al., 2018) or ^{14}C ages from the box cores (Colman et al., 1996).

2.2. Sample Preparation and Analysis

Sediments were freeze dried and weighed prior to homogenization. Since samples from cores 333-PC2, 340-TC1, and 340-PC1 were archived cubes used for paleomagnetic analysis (Peck et al., 1994), DBD was readily calculated from sample weight and volume. Lipids were extracted by an accelerated solvent extractor (ASE) 350 using 2:1 dichloromethane: methanol with the following conditions: oven temperature 100°C, heating time to 5 min, 4 × 10-min static cycles with a rinse volume of 150%, and an N_2 purge time to 120 s. We used this more polar solvent mixture than the typical 9:1 dichloromethane: methanol to recover more polar molecules (e.g., saccharides and alcohols) from our sediment samples. The more polar solvent schedule should not influence the relative distributions of GDGTs in our samples (see Auderset et al. (2020); Powers et al. (2010)).

Total lipid extracts were spiked with 100 μL of a general recovery standard (20.5 ng/μL 5α-androstane, 20.5 ng/μL stearyl stearate, 20.5 ng/μL 1,1′-binapthyl, 20.5 ng/μL cis-11-eicosenoic acid, 20.5 ng/μL 19-methyleicosenoic acid, 20.5 ng/μL $C_{20:1}$ Δ11-eicosenol, and 20.5 ng/μL 5α-androstan-3β-ol), desulfurized by sequential addition of activated copper wire, and evaporated under N_2 prior to separation on a 0.5 g dry-packed LC-NH_2 column to separate neutral (4 mL 2:1 dichloromethane: isopropanol), acid (4 mL 4% acetic acid in diethyl ether), and polar (4 mL methanol) fractions. Neutral and polar fractions were recombined and again dried under N_2 prior to elution on a wet-packed silica gel (0.5 g, 60 Å, 70–230 mesh, Millipore) column with 3 mL hexanes (apolar/aliphatic), 4 mL dichloromethane (semi-polar/aromatic), and 4 mL methanol (polar/alcohols). The polar/alcohols (methanol) fraction was further separated over alumina oxide (0.85 g, J.T. Baker, 0537-01) by elution of 4 mL 9:1 hexane: dichloromethane, 4 mL 1:1 dichloromethane: methanol (containing GDGTs), and 4 mL 100% methanol. The 1:1 dichloromethane: methanol fraction was then dried over N_2 and shipped to Brown University, where the GDGTs were analyzed on an Agilent/Hewlett Packard 1,100 series liquid chromatograph mass spectrometer (LC-MS) using two UHPLC columns (BEH HILIC columns, 2.1 × 150 mm, 1.7 μm, Waters) in series using the protocol of Hopmans et al. (2016). Prior to analysis, samples were passed through a 0.45 μm filter and spiked with a known quantity of a C_{46} glycerol trialkyl glycerol tetraether (GTGT) internal standard (Huguet et al., 2006). Selective ion monitoring was used to measure *m/z* 1302, 1300, 1298, 1296, 1292, 1050, 1048, 1046, 1036, 1034, 1032, 1022, 1020, 1018, and 744. Peak areas were quantified manually using the Chemstation software. Concentrations of individual GDGT molecules are reported in nanograms per gram of sediment (ng/g sed), assuming a 1:1 relationship between the response factor of the C_{46} GTGT and the individual brGDGTs (Huguet et al., 2006). While this assumption may not capture the exact response factors of the individual brGDGTs, it is sufficient for understanding the relative concentrations of different brGDGTs in this sample set.

2.3. Calculations

We describe brGDGT distributions via IR_{6Me} (Equation 1), the isomer ratio of five-to six-methyl brGDGTs (Dang, Xue, et al., 2016; Dang, Yang, et al., 2016). As IR_{6Me} approaches 1, the larger the proportion of six-methyl brGDGTs in each sample:

$$IR_{6Me} = \frac{(IIa' + IIb' + IIc' + IIIa' + IIIb' + IIIc')}{(IIa + IIa' + IIb + IIb' + IIc + IIc' + IIIa + IIIa' + IIIb + IIIb' + IIIa + IIIa')} \tag{1}$$

We describe the cyclization of brGDGTs with the CBT′ index (Equation 2) (De Jonge et al., 2014):

$$CBT' = \log_{10}\left(\frac{Ic + IIa' + IIb' + IIc' + IIIa' + IIIb' + IIIc'}{Ia + IIa + IIIa}\right) \tag{2}$$

The degree of methylation of brGDGTs was related to temperature by the MBT'_{5Me} index (Equation 3) (De Jonge et al., 2014):

$$MBT'_{5Me} = \frac{(Ia + Ib + Ic)}{(Ia + Ib + Ic + IIa + IIb + IIc + IIIa)} \tag{3}$$

We report and analyze the concentration of branched GDGTs in our samples as described by the sum of the abundances of the branched GDGTs (Equation 4):

$$\begin{aligned}\sum brGDGTs = {} & [Ia] + [Ib] + [Ic] + [IIa] + [IIa'] + [IIb] + [IIb'] + [IIc] + [IIc'] + [IIIa] \\ & + [IIIa'] + [IIIb] + [IIIb'] + [IIIc] + [IIIc']\end{aligned} \tag{4}$$

We report values of the branched index of tetraethers (BIT) described by Equation 5, which was once considered a useful metric for identifying terrigenous organic matter input to lacustrine and marine sediments (Hopmans et al., 2004):

$$\mathrm{BIT} = \frac{(\mathrm{I}a + \mathrm{II}a + \mathrm{II}a' + \mathrm{III}a + \mathrm{III}a')}{(\mathrm{I}a + \mathrm{II}a + \mathrm{II}a' + \mathrm{III}a + \mathrm{III}a' + \mathrm{Crenarchaeol})} \tag{5}$$

Whenever the full suite of isoprenoid and branched GDGTs was quantifiable, we classified sample brGDGT provenance via the BIGMaC algorithm (Martínez-Sosa et al., 2023), a machine learning algorithm that classifies samples as soil, peat, lake, or marine provenance based on the fractional abundances of isoprenoid and branched GDGTs.

2.4. Previous Temperature Calibrations

We utilized several published methods to translate $\mathrm{MBT'}_{5\mathrm{Me}}$ or the relative abundances of brGDGTs in Lake Baikal samples to temperature. First, we used the Bayesian calibration of $\mathrm{MBT'}_{5\mathrm{Me}}$ in lake sediments to mean months above freezing temperature (MAF) by Martínez-Sosa et al. (2021).

$$\mathrm{MBT'}_{5\mathrm{Me}} = 0.030(\pm 0.001)\,\mathrm{MAF} + 0.075(\pm 0.012) \tag{6}$$

In addition, we used the full set calibration of Raberg et al. (2021), which estimates months above freezing temperature from the fractional abundances of select brGDGTs calculated from the full suite of brGDGT molecules.

$$\begin{aligned}\mathrm{MAF} = &-8.06(\pm 1.56) + 37.52(\pm 2.35)\,[\mathrm{I}a] - 266.83(\pm 96.61)\,[\mathrm{I}b]^2 + 133.42(\pm 19.51)\,[\mathrm{I}b] \\ &+ 100.85(\pm 9.27)\,[\mathrm{II}a']^2 - [\mathrm{II}a']^2 + 58.15(\pm 10.09)\,[\mathrm{III}a']^2 + 12.79(\pm 10.09)[\mathrm{III}a]\end{aligned} \tag{7}$$

We also applied the methylation set calibration of Raberg et al. (2021), which incorporates the fractional abundances of select individual brGDGTs calculated within sets of brGDGTs with the same number of cyclopentane rings and the same methylation positions in a multivariate regression to months above freezing temperature.

$$fxy_{\mathrm{meth}} = \frac{xy}{\sum_{n=\mathrm{I}}^{\mathrm{III}} ny}\,; fxy'_{\mathrm{meth}} = \frac{xy'}{\sum_{n=\mathrm{II}}^{\mathrm{III}} ny'} \tag{8}$$

$$\begin{aligned}\mathrm{MAF} = &\,92.9(\pm 15.98) + 63.84(\pm 15.58)\,[\mathrm{I}b_{\mathrm{meth}}]^2 - 130.51(\pm 30.73)\,[\mathrm{I}b_{\mathrm{meth}}] - 28.77(\pm 5.44)\,[\mathrm{II}a_{\mathrm{meth}}]^2 \\ &- 72.28(\pm 17.38)\,[\mathrm{II}b_{\mathrm{meth}}] - 5.88(\pm 1.36)\,[\mathrm{II}c_{\mathrm{meth}}]^2 + 20.89(\pm 7.69)\,[\mathrm{III}a_{\mathrm{meth}}]^2 \\ &- 40.54(\pm 5.89)\,[\mathrm{III}a_{\mathrm{meth}}] - 80.47(\pm 19.19)\,[\mathrm{III}b_{\mathrm{meth}}]\end{aligned} \tag{9}$$

We also used the mixing model approach proposed by Wang et al. (2024) to reconstruct the bacterial growth temperature in samples with mixed contributions of brGDGTs from 5-methyl and 6-methyl brGDGT-producing bacteria.

$$\begin{aligned}([\mathrm{I}a] + [\mathrm{I}b] + [\mathrm{I}c]) = &\frac{A \times T + B}{1 - (A \times T + B)}([\mathrm{II}a] + [\mathrm{II}b] + [\mathrm{II}c] + [\mathrm{III}a] + [\mathrm{III}b] + [\mathrm{III}c]) \\ &+ \frac{C \times T + D}{1 - (C \times T + D)}([\mathrm{II}a'] + [\mathrm{II}b'] + [\mathrm{II}c'] + [\mathrm{III}a'] + [\mathrm{III}b'] + [\mathrm{III}c'])\end{aligned} \tag{10}$$

A, B, C, and D are constants derived from lacustrine suspended particulate matter data sets and T is the growth temperature (Wang et al., 2024).

2.5. Compilation of Existing brGDGT and Environmental Data

We leveraged the recent global brGDGT lacustrine surface sediment data set of Zhao et al. (2023), who compiled data from Baxter et al. (2019), Cao et al. (2020), Dang et al. (2018), Li et al. (2017), Liang et al. (2022), Martínez-Sosa et al. (2021), Ning et al. (2019), Qian et al. (2019), Raberg et al. (2021), Russell et al. (2018), Wang et al. (2021), Weber et al. (2018), Zhao et al. (2021). We expanded the Zhao et al. (2023) data set with subsequently published brGDGT measurements from lakes in Switzerland and Alaska (Bauersachs et al., 2024; Otiniano et al., 2023). In addition, we utilized the soil brGDGT data set assembled by Dearing Crampton-Flood et al. (2020), who compiled data from De Jonge et al. (2014), Ding et al. (2015), Lei et al. (2016), Wang et al. (2016), Xiao et al. (2015), and Yang et al. (2015). We also incorporated published paired data sets from lake sediments and lake catchments (Raberg, Flores, et al., 2022; Wang et al., 2023; Weber et al., 2018; Zhao et al., 2021) alongside a lake sediment and catchment data set we assembled from our own measurements of surface sediments at Lake Baikal and published data from moss polsters (Dugerdil et al., 2020) and riverine suspended particulate matter (De Jonge et al., 2015) in Lake Baikal's catchment. All compiled data were collected using protocols that separate 5 -and-6-methyl brGDGTs (De Jonge et al., 2013; Hopmans et al., 2016).

We assigned months above freezing (middle and high latitude lakes) and mean annual surface air temperatures (tropical lakes) to the new samples in the global lacustrine brGDGT surface sediment data set from the WorldClim version 2.1 30-s resolution data set (Fick & Hijmans, 2017), which incorporates data from the years 1970–2000, following the method of Zhao et al. (2023). We consider middle and high latitude lakes to be all lakes outside 30°S–30°N and tropical lakes as all lakes within 30°S–30°N. Since there are not surface air temperatures in the WorldClim data set over Lake Baikal, our surface sediment samples were excluded from the lacustrine temperature calibration data set (12 of 648 samples excluded).

3. Results

3.1. Branched GDGT Distributions in Lake Baikal Sediments

The distribution of brGDGTs in Lake Baikal sediments is dominated by IIIa and IIIa′ (Figures 1c and 1d, IIIa′ refers to the 6-methyl brGDGT isomer). We did not observe IIIa′′ in Lake Baikal sediments. IIIa is expected to be abundant given the cold climate of the Lake Baikal region and the inverse temperature dependence of the abundance of brGDGT IIIa found by previous studies (De Jonge et al., 2014; Russell et al., 2018; Zhao et al., 2023). Greater abundance of brGDGT IIIa′ is primarily associated with decreasing pH in soils (De Jonge et al., 2014).

We were not able to quantify the full suite of isoprenoid GDGTs in all samples from Lake Baikal necessary for application of the BIGMaC algorithm due to the low concentration of iGDGTs in many samples. However, samples in which all the iGDGTs and brGDGTs were quantifiable were classified as lacustrine in origin by BIGMaC (Martínez-Sosa et al., 2023).

We observed changes in MBT'_{5Me} in Baikal sediments that correlate with climate-driven lithologic variations. The dry bulk density of Lake Baikal sediments primarily reflects its biogenic silica content (Figure S3a in Supporting Information S1), which is an indicator of relative climate change at Lake Baikal (Colman et al., 1995; Prokopenko et al., 2006; Williams et al., 1997). Diatomaceous ooze, characterized by high biogenic silica content and lower dry bulk density, was deposited during warm periods, while silty clay with higher dry bulk density and low biogenic silica content was deposited during cold periods (Figure S3a in Supporting Information S1). Prior to 50 Ka, high MBT'_{5Me} values and warm reconstructed MAF paleotemperatures in Lake Baikal sediments tended to co-occur with diatomaceous oozes and lower MBT'_{5Me} values and cold reconstructed MAF paleotemperatures with clays (Figures 2a and 3a). However, in the last 50 Ka, there are many high MBT'_{5Me} values that coincide with clays, suggesting anomalously warm conditions during the Last Glacial Maximum (Figures 2a and 3a, 29–14 Ka). These high MBT'_{5Me} values are accompanied by relatively low brGDGT concentration (Figure 2b), high IR_{6Me} (>0.4, Figure 2c) and high CBT′ (Figure 2d) values but do not appear different from the older samples in their BIT values or when applying the BIGMaC algorithm (Figure S4 in Supporting Information S1). Samples $IR_{6Me} > 0.4$ occur in cores 333-PC2, 340-TC1, and VER92/2-GC24 (Figure S5 in Supporting Information S1).

Given the correspondence of high MBT'_{5Me} (>0.4), IR_{6Me} (>0.4), and CBT′ (>0) values during the past 50 Ka at Lake Baikal (Figure 2a), we attempted to reconstruct paleotemperatures using methods that account for the potential influence of 6-methyl brGDGTs on temperature estimates (Raberg et al., 2021; Wang et al., 2024). A mixing model method (Wang et al., 2024) and "full set" and "methylation set" calibrations (Raberg et al., 2021) yielded anomalously warm paleotemperatures of the past 50 Ka (Figures 3c, 3e, and 3g, note glacial temperatures equivalent to much of the Holocene). For the mixing model and full set methods, paleotemperature estimates vary with IR_{6Me}: samples with $IR_{6Me} \leq 0.4$ have significantly lower reconstructed paleotemperatures than samples with $IR_{6Me} \geq 0.55$ in both glacial clays and interglacial diatomaceous oozes (Figures 3d and 3h, compare to

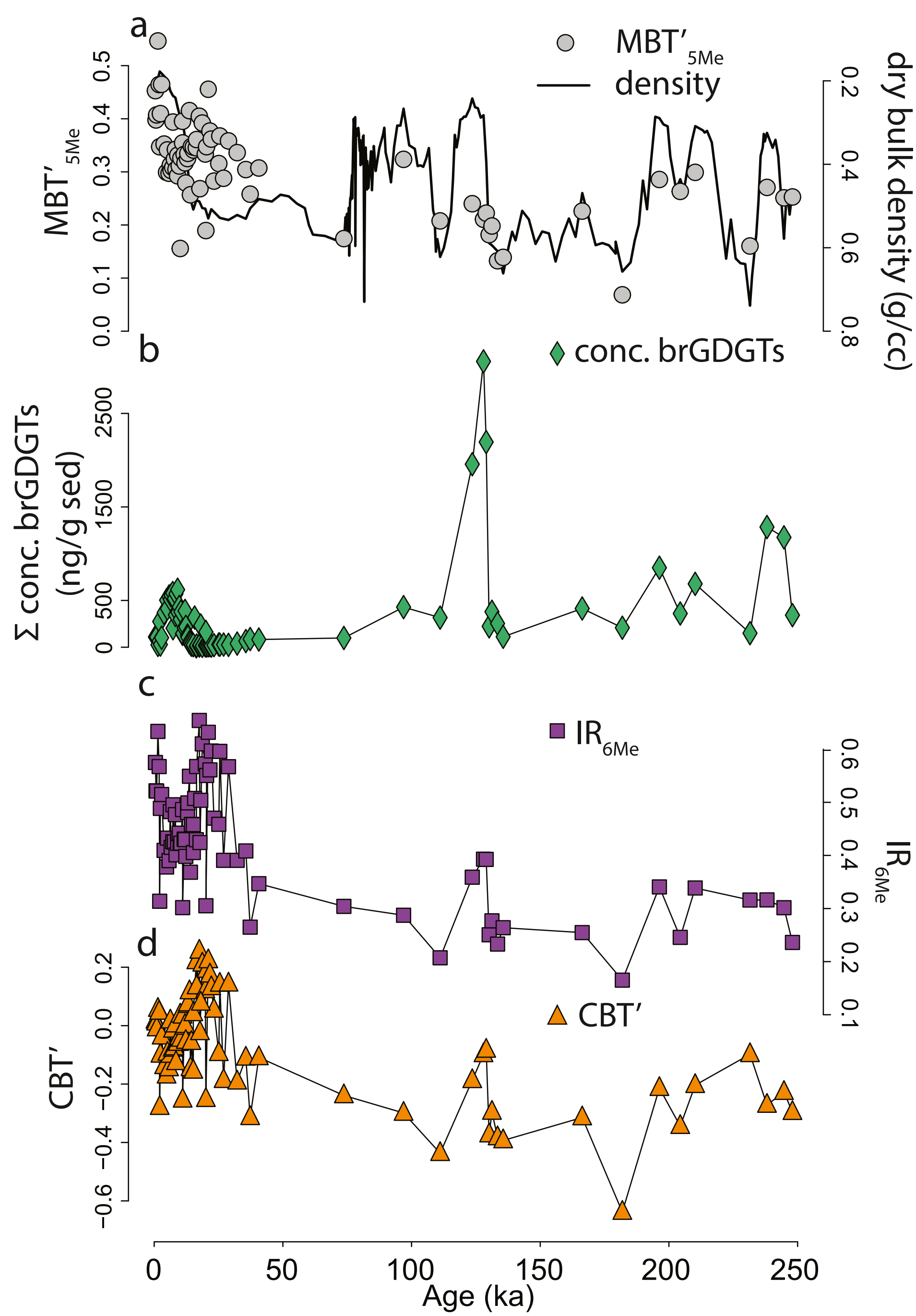

Figure 2. BrGDGT indices from Lake Baikal over the last 250 Ka. (a) Timeseries of dry bulk density (black line) and MBT'_{5Me} values (gray circles) from Lake Baikal covering the past 250 Ka. (b) The total concentration of brGDGTs. (c) IR_{6ME} values. (d) CBT′ values. Note the coincidence of high MBT'_{5Me}, low concentration of brGDGTs, high IR_{6Me}, and high CBT′.

MBT'_{5Me} in Figure 3b). Although the methylation set method addresses this issue, this method instead increases the apparent amplitude of glacial-interglacial temperature change in samples with high IR_{6Me} (Figure 3f and Figure S6 in Supporting Information S1). When viewed in timeseries, this gives the impression of a far larger reconstructed MAF paleotemperature difference between the Last Glacial Maximum and Holocene than MIS 6 and 5 (Figure S7 in Supporting Information S1), which we suspect is unlikely in view of the global similarity of these glacial-interglacial climate cycles (Lisiecki & Raymo, 2005) and previous studies of this interval at Lake

10.1029/2024GC012069

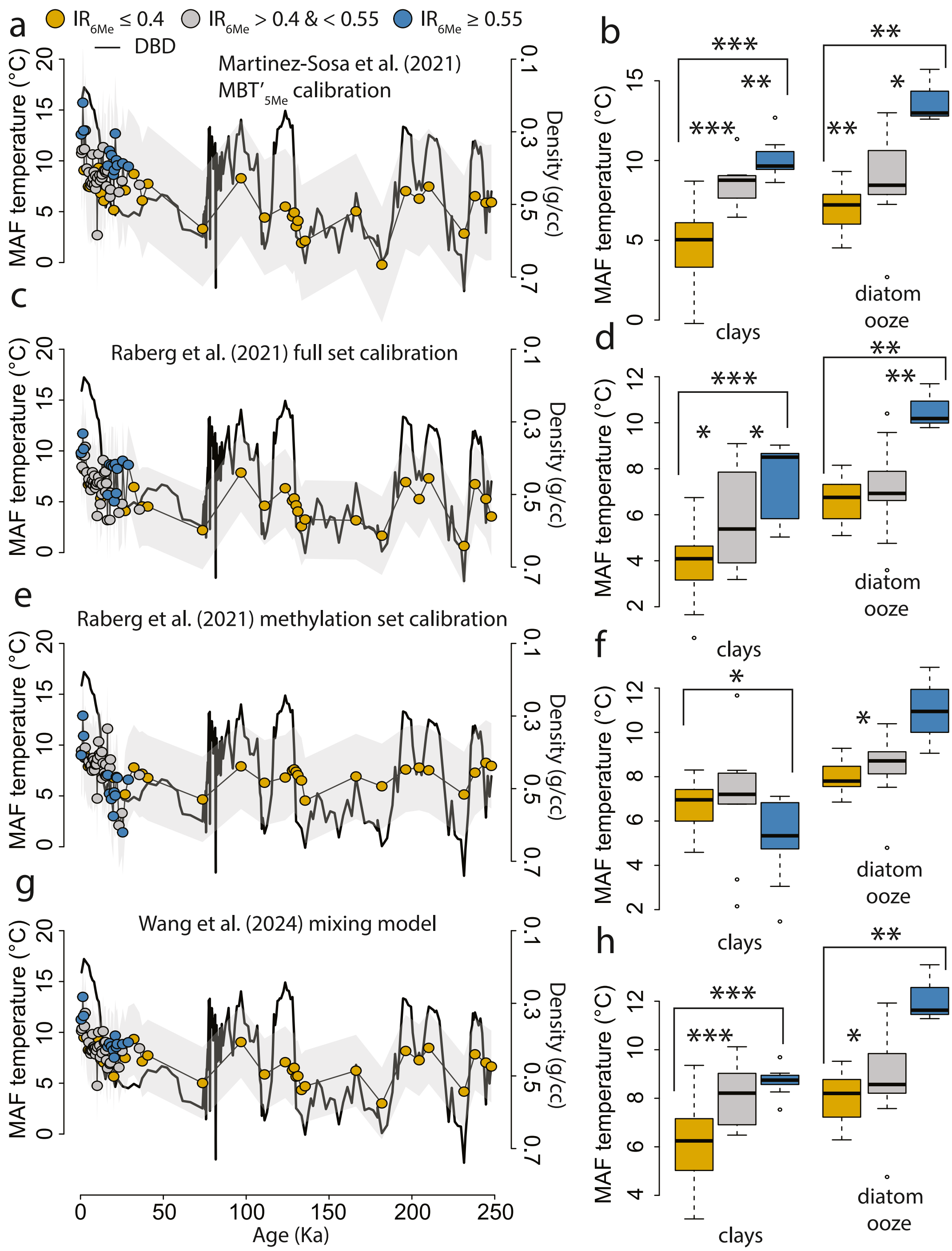

Figure 3. Lake Baikal brGDGT paleotemperature estimates using the methods of Martínez-Sosa et al. (2021), Raberg et al. (2021), and Wang et al. (2024). (a) Timeseries of reconstructed paleotemperatures using the MBT'_{5Me} calibration of Martínez-Sosa et al. (2021). (b) Box and whisker plots of paleotemperatures reconstructed with the method of Martínez-Sosa et al. (2021). Samples are grouped by IR_{6Me} as in (a) and separated by lithology as a proxy for climate state, with samples of a dry bulk density ≥ 0.4 g*cm^{-3} classified as clays. (c) Same as (a) using the full set method of Raberg et al. (2021). (d) Same as (b) using the full set method of Raberg et al. (2021). (e) Same as (a) using the methylation set calibration of Raberg et al. (2021). (f) Same as (b) using the methylation set calibration of Raberg et al. (2021). (g) Same as (a) using the mixing model method of Wang et al. (2024). (h) Same as (b) using the mixing model method of Wang et al. (2024). In (a–h), samples are grouped by IR_{6Me}: gold—$IR_{6Me} \leq 0.4$; gray—$IR_{6Me} > 0.4$ & <0.55; blue—$IR_{6Me} \geq 0.55$. In (a, c, e, g), shading shows the 95% uncertainty in estimated paleotemperatures. In (b, d, f, and h), line, box, and whiskers indicate the median, 1st and 3rd quartiles and minimum and maximum values within 1.5 times the interquartile range, with outliers (>1.5 times the interquartile range) shown as individual points. * *t*-test *p*-value <0.05, ** *t*-test *p*-value <0.01, *** *t*-test *p*-value <0.001 where the alternative hypothesis is that estimated temperatures in clays are less than those in diatomaceous oozes.

10.1029/2024GC012069

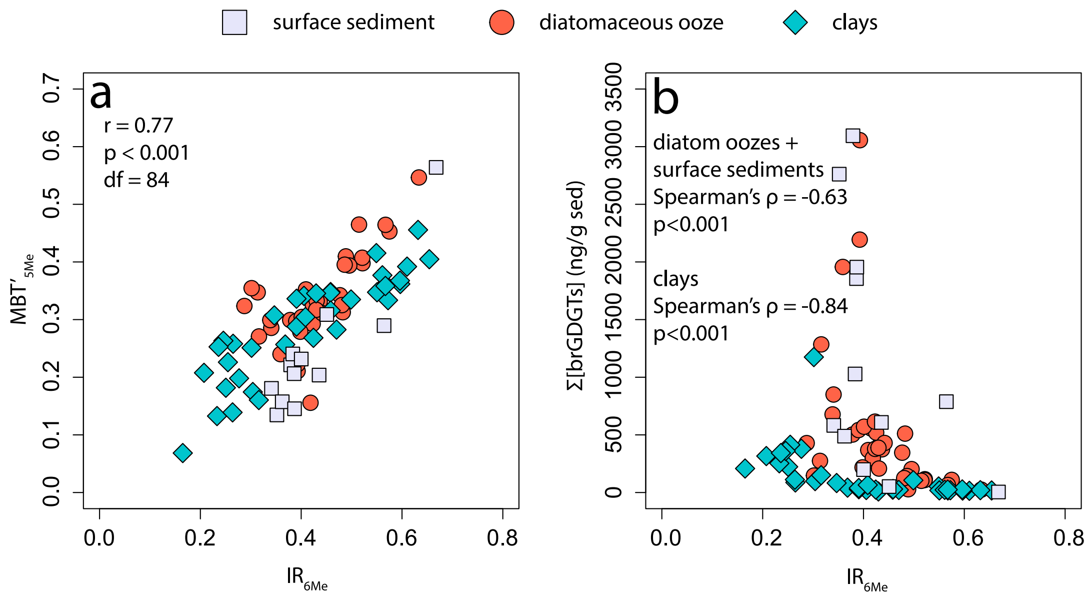

Figure 4. IR_{6Me} is correlated with MBT'_{5Me} and branched GDGT concentration in Lake Baikal sediments. (a) Correlation between IR_{6Me} and MBT'_{5Me} in downcore and core top sediments. (b) Correlation between IR_{6Me} and the sum of the concentration of the branched GDGTs. Samples with a dry bulk density ≥ 0.4 g*cm^{-3} are classified as clays.

Baikal based on pollen and bulk sedimentology (BDP-99 Members, 2005; Colman et al., 1995; E. B. Karabanov et al., 2000; Khursevich et al., 2001; Peck et al., 1994; Prokopenko et al., 2006; Tarasov et al., 2005, 2009). Notably, each method reconstructs significant differences in MAF paleotemperatures between glacial clays and interglacial diatomaceous oozes in samples grouped by IR_{6Me} (Figure S8 in Supporting Information S1).

MBT'_{5Me} is moderately related to IR_{6Me} in sediment core and surface sediment samples at Lake Baikal (Figure 4a; $r = 0.77$, $p < 0.001$, df = 84). IR_{6Me} and the concentration of branched GDGTs in Lake Baikal samples are significantly anticorrelated (Figure 4b; Spearman's $\rho = -0.63$, $p < 0.001$ in surface sediments and diatom oozes; Spearman's $\rho = -0.84$, $p < 0.001$ in clays). The samples separate into two distinct populations based on lithology and brGDGT concentration: clays (Figure 4b, diamonds) and diatomaceous oozes and surface sediments (Figure 4b, circles and squares). We also observed a significant relationship between MBT'_{5Me} and CBT′ in Lake Baikal sediments (Figure S9 in Supporting Information S1, adj. $r^2 = 0.42$, $r = 0.65$, $p < 0.001$, df = 84). We see no clear clustering or correlation between individual brGDGTs and individual iGDGTs (Figure S10 in Supporting Information S1).

3.2. Branched GDGT Distributions in Globally Distributed Lakes

We analyzed the relationship between IR_{6Me} and MBT'_{5Me} in the global lacustrine surface sediment data set (Figure 5). There is a weak but significant correlation between MAF temperature and IR_{6Me} in globally distributed lake surface sediments in which IR_{6Me} is likely to be higher with warmer MAF temperatures (adj. $r^2 = 0.09$, $r = 0.31$, $p < 0.001$, df = 635, Figure 5b). In regressions of MAF on MBT'_{5Me}, there is a group of samples with $IR_{6Me} \geq 0.55$ between 5 and 15°C MAF that have MBT'_{5Me} values that are higher than expected from the MAF and line of best fit (Figure 5c black arrow) as predicted by Wang et al. (2024). This group of samples is only a subset of the larger group of samples with $IR_{6Me} \geq 0.55$ (Figure 5c). We also observed a large cluster of intermediate and high IR_{6Me} lakes in midlatitude Asia, North America, and equatorial East Africa (Figures 5a, Figures S11b and 11c in Supporting Information S1).

The group of samples with $IR_{6Me} \geq 0.55$ and MBT'_{5Me} values 0.2–0.4 higher than expected (Figure 5c arrow) led us to systematically investigate whether the relationship between MBT'_{5Me} and environmental temperature varies in samples with different IR_{6Me} values. Data from tropical and middle to high latitude lakes were analyzed separately because of the differing temperature seasonality in the low versus middle to high latitudes that could lead to different calibration relationships (Cao et al., 2020; Raberg et al., 2021; Zhao et al., 2023). We grouped samples by IR_{6Me} into bins 0.2 IR_{6Me} units wide and iteratively regressed the binned samples to MAF, which in

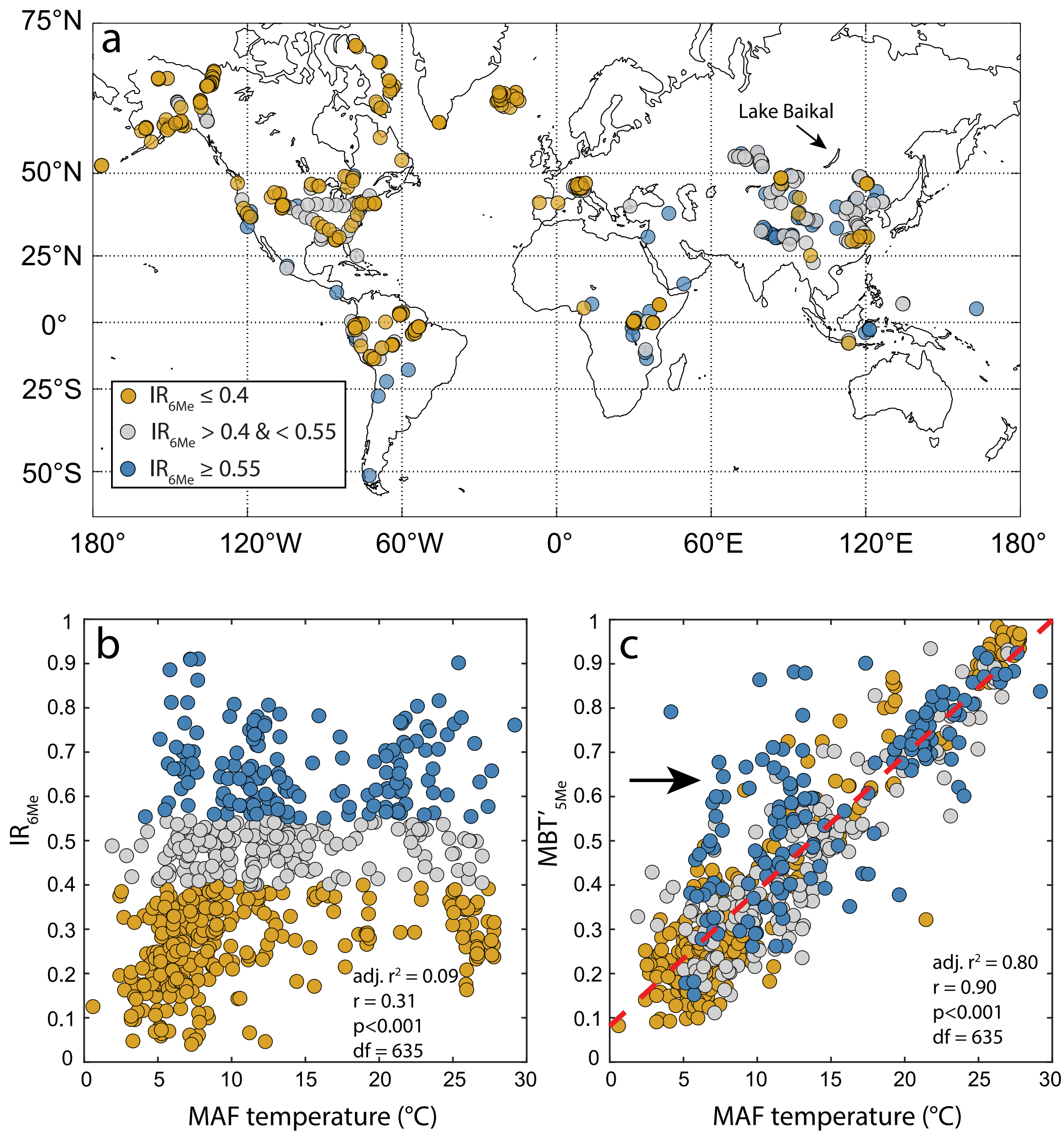

Figure 5. Branched GDGT distributions in globally distributed lacustrine sediments. (a) Map showing locations of brGDGT lacustrine sedimentary surficial samples. Basemap is from the M_Map MATLAB package (Pawlowicz, 2020). (b) Scatterplot of MAF temperature and IR_{6Me}. (c) Scatterplot of MAF temperature and MBT'_{5Me}. The red dashed line is the fitted line determined by Ordinary Least Squares regression. Black arrow shows a cluster of higher-than-expected MBT'_{5Me} values with $IR_{6Me} > 0.55$. Data point colors in b and c correspond to the IR_{6Me} values in (a).

the tropics is equivalent to mean annual air temperature (MAAT). The bin of samples was shifted by 0.01 IR_{6Me} units at each iteration, generating a continuous profile of regression parameters across the lacustrine surface sample data set (Figure 6). The uncertainty in the regression parameters (Figure 6, light blue shading) increases with a smaller sample number or with a weaker fit to the data.

We observed a systematic change in the values of both the intercept and slope of MBT'_{5Me}-temperature regressions in middle and high latitude lakes with IR_{6Me} (Figures 6a and 6b). When the IR_{6Me} bin midpoint is less than approximately 0.4, the regression intercept is relatively low (~2–3°C) and the slope is relatively high (~15–20°C/MBT'_{5Me}) (Figures 6a and 6b). Conversely, when the IR_{6Me} bin midpoint is greater than approximately 0.55, the regression intercept is relatively high (~5–6°C) and the slope low (~10°C/MBT'_{5Me}) (Figures 6a and 6b). We did not observe the same systematic change in the regression coefficients in tropical lakes (Figures 6c and 6d) except for a small group of samples with IR_{6Me} of 0.6–0.7. We tested the robustness of this finding by

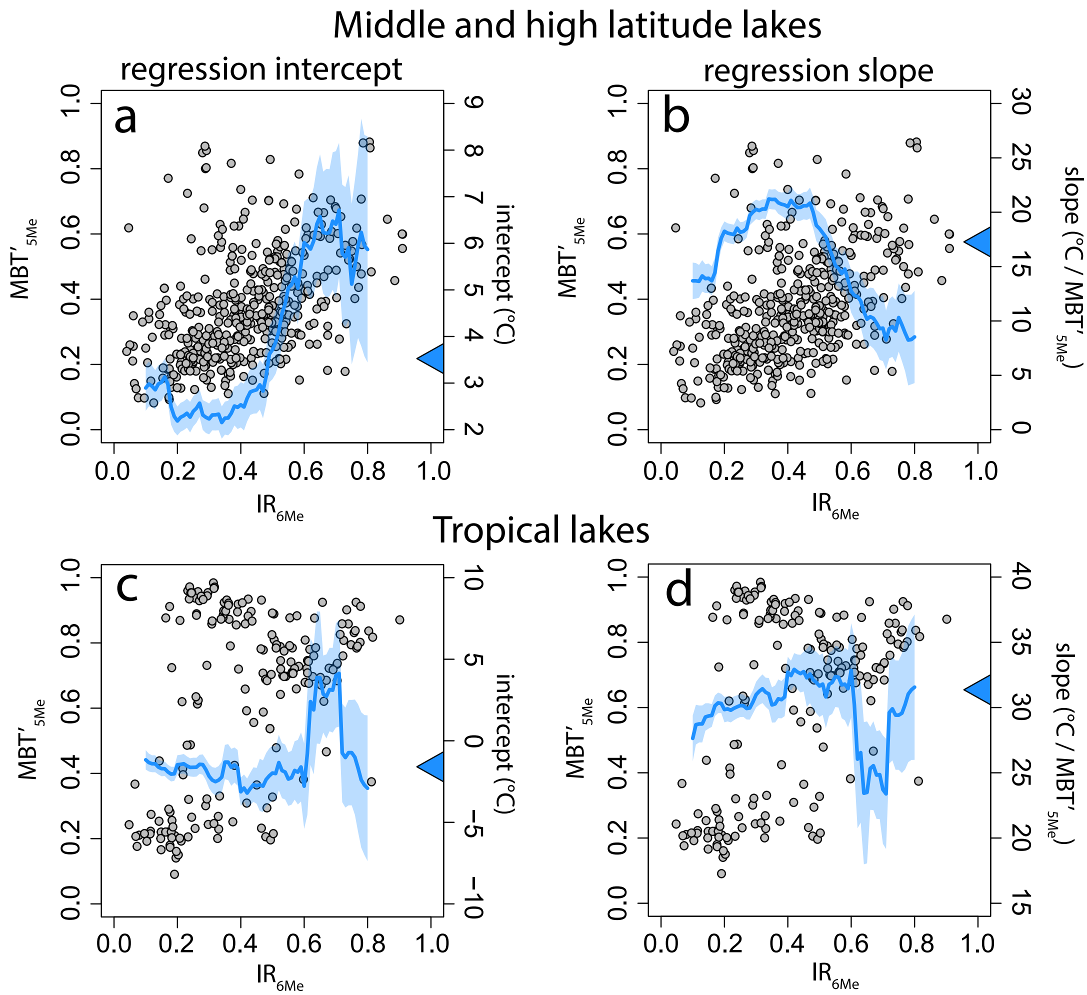

Figure 6. MBT'_{5Me}-temperature regression coefficients with IR_{6Me} in mid to high latitude and tropical lakes. (a) Change in MBT'_{5Me}-MAF regression intercept (blue line and shading) with IR_{6ME} (gray points) in mid and high latitude lakes. Blue triangle shows the intercept of the regression between MBT'_{5Me} and MAF in all mid and high latitude lakes. (b) Change in MBT'_{5Me}-MAF regression slope with IR_{6Me} in mid and high latitude lakes. (c) Change in MBT'_{5ME}-MAAT regression intercept in tropical lakes. Blue triangle shows the intercept of the regression between MBT'_{5Me} and MAAT in all tropical lakes. (d) Change in MBT'_{5Me}-MAAT regression slope with IR_{6Me} in tropical lakes. Shading in (a–d) shows 1σ standard error of the regression coefficients. Blue triangles in each panel show the value of the MBT'_{5Me}-MAF or MAAT regression slope or intercept for all the samples in that panel.

leveraging the strong correlation between IR_{6Me} and CBT′ (Figure S12 in Supporting Information S1) to conduct a parallel analysis of how MBT'_{5Me}-temperature regression parameters change with variations in CBT′ (Figure S13 in Supporting Information S1). While we observe analogous changes in MBT'_{5Me}-temperature regression parameters with increasing CBT′ in middle and high latitude lakes (Figures S13a and S13b in Supporting Information S1), we do not observe such systematic changes in tropical lakes (Figures S13c and S13d in Supporting Information S1). Regression slopes inferred in the middle and high latitude lakes data set are never equivalent to the slopes of the tropical lakes data set (Figure S14b in Supporting Information S1) and the regression intercepts are only within error of each other within the 0.6–0.7 IR_{6Me} range (Figure S14a in Supporting Information S1).

Principal component analysis (PCA) of the global lacustrine surface sediment data set provides further insight into the extent to which the middle to high latitude and tropical lakes brGDGT samples exhibit non-thermal influences on brGDGT methylation (Figure 7). PC1 explains 45.8% and PC2 33.8% of the variance in the middle and high latitude lakes data set (Figure 7a). Middle and high latitude lake PC1 is correlated to MAF temperature ($r = 0.93$) and MBT'_{5Me} ($r = 0.96$), while PC2 is correlated to IR_{6Me} ($r = -0.85$) and CBT′ ($r = -0.97$, Figure 7b). By comparison, PC1 explains 77.6% of the variance in the tropical lakes data set and is

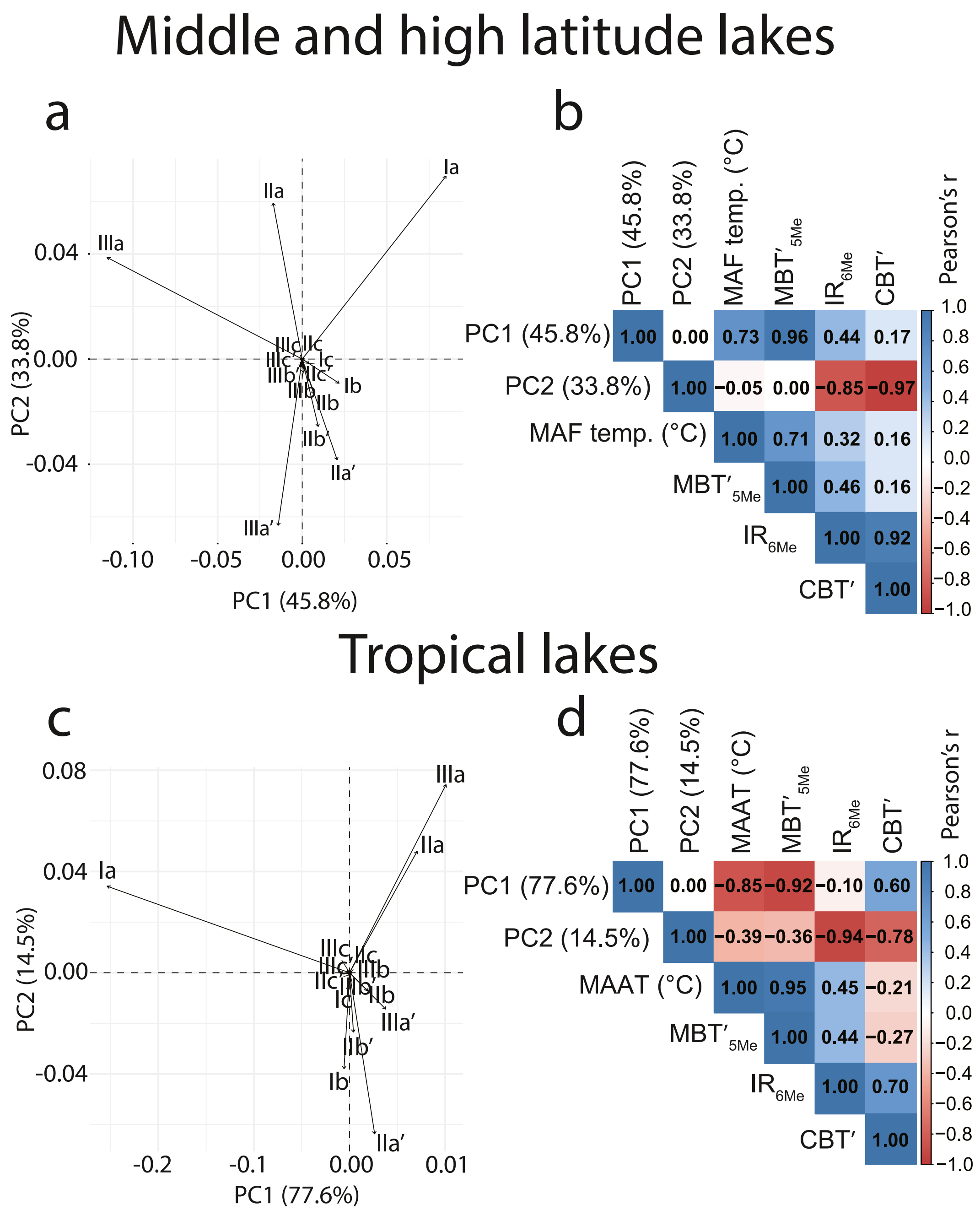

Figure 7. Principal component analysis of the global lacustrine surface sediment data set. (a) Loadings of individual brGDGTs on PC1 and PC2 in middle and high latitude lakes. (b) Correlation matrix showing Pearson's r between PC1, PC2, MAF temperature, and brGDGT indices in the middle and high latitude lakes data set. (c) Loadings of individual brGDGTs on PC1 and PC2 in tropical lakes. (d) Correlation matrix showing Pearson's r between PC1, PC2, MAAT, and brGDGT indices in the tropical lakes data set.

correlated with MAAT ($r = -0.85$) and MBT'_{5Me} ($r = -0.92$), while PC2 explains 14.5% of the variance and is correlated to IR_{6Me} (-0.94) and CBT′ (-0.78, Figures 7c and 7d). In both the data sets, it appears that PC1 reflects temperature or methylation while PC2 reflects isomerization, and cyclization or the process(es) controlling those aspects of brGDGT distributions (cf. Parish et al., 2023). The lower explanatory power of PC1 (temperature) and greater explanatory power of PC2 (possible drivers discussed in Section 4.1) in the middle and high latitude lakes data set compared to the tropical lakes data set supports the idea that the middle and high latitude lakes surface sediment brGDGT data are more prone to non-thermal influences than the tropical lakes data.

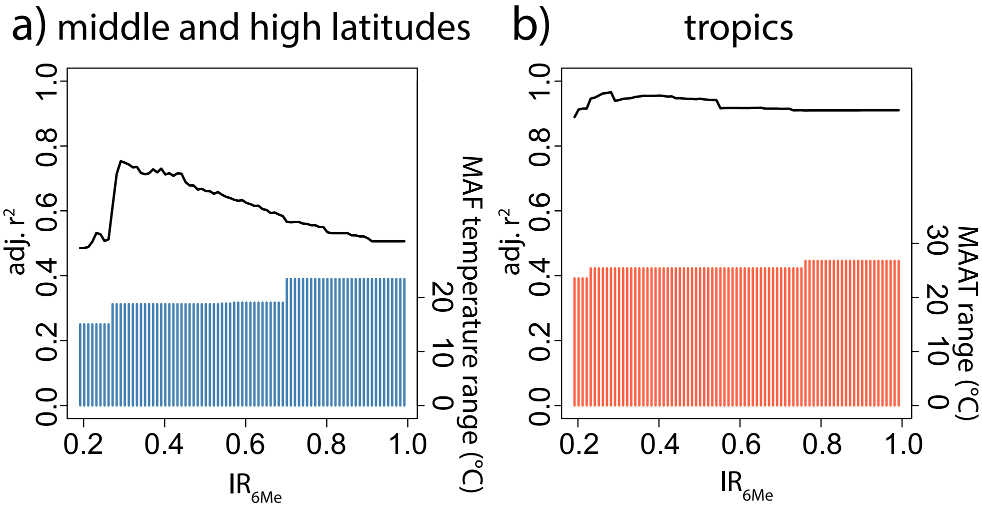

Figure 8. Change in adjusted r^2 of MBT'_{Me}-temperature regression with IR_{6Me} cutoff. (a) Change in adjusted r^2 of the regression between MBT'_{5Me} and MAF temperature in middle and high latitude lakes with IR_{6Me} cutoff systematically increased from 0.2 to 1.0. Blue bars show the MAF temperature range sampled by each regression. (b) Change in adjusted r^2 of the regression between MBT'_{5Me} and MAAT in tropical lakes with IR_{6Me} cutoff threshold. Red bars show the MAAT range sampled by each regression. In (a and b), adj. r^2 values were determined by selecting samples with IR_{6Me} less than the given cutoff value and then regressing the MBT'_{5Me} value of those samples to their assigned temperature. The IR_{6Me} cutoff was systematically increased by 0.01 at every iteration.

Our observations suggest that brGDGT isomerization (IR_{6Me}) characterizes processes that influence the relationship between MBT'_{5Me} and temperature (Figure 6). This may account for the group of samples with $IR_{6Me} > 0.55$ and high MBT'_{5Me} between 5 and 15°C MAF contributing to scatter in the regression between MAF and MBT'_{5Me} in global lakes (Figure 5c). Cyclization (CBT′) of brGDGTs also appears to capture this process (Figure S13 in Supporting Information S1), which is expected since IR_{6Me} and CBT′ are strongly related in lacustrine sediments (Figure S12 in Supporting Information S1, adj. $r = 0.78$, see also Dang, Xue, et al., 2016; Dang, Yang, et al., 2016; Raberg et al., 2021).

3.3. Filtering Samples by IR_{6Me} Improves MBT'_{5Me} Temperature Calibrations

We focused our subsequent data analysis on IR_{6Me} because the middle and high latitude lake MBT'_{5Me} data are more evenly distributed in IR_{6Me} space, enabling a more thorough investigation of the IR_{6Me} binning exercise in Figure 6 than the CBT′ binning exercise in Figure S13 in Supporting Information S1. In particular, we tested whether grouping lake sediment samples by IR_{6Me} improves the statistical strength of lacustrine MBT'_{5Me}-temperature calibrations. The correlation statistic (adjusted r^2) of the regression between MBT'_{5Me} and MAF temperature in middle and high latitude lakes systematically improves when imposing a lowering IR_{6Me} cutoff threshold on the data until an IR_{6Me} value of 0.27 (Figure 8a), at which point the sampled MAF temperature range narrows and the degrees of freedom are reduced (Figure 8a, Figure S15 in Supporting Information S1). By comparison, there is relatively little change in the regression parameters between MBT'_{5Me} and MAAT in tropical lakes with different IR_{6Me} values (Figure 8b).

This analysis and our investigation of the variation of MBT'_{5Me}-temperature regression coefficients with IR_{6Me} suggest that removing samples with high IR_{6Me} will improve the statistical power of the MBT'_{5Me}-MAF temperature calibration in middle and high latitude lakes (Figures 6 and 8). We chose an IR_{6Me} cutoff threshold of 0.4 as a conservative value based on our analysis of slope/intercept variability (Figure 6) and regression fit (Figure 8). This cutoff minimizes any potential non-thermal influence on the global MBT'_{5Me}-temperature calibration; it is possible that a higher or lower IR_{6Me} cutoff value may be more appropriate on a regional or lake system basis (e.g., Bauersachs et al., 2024 who used an IR_{6Me} cutoff value of 0.5). We observe a substantial improvement in the regression statistics between MBT'_{5Me} and MAF temperature in the combined mid and high latitude lakes data set when samples with an $IR_{6Me} > 0.4$ are removed (Figures 9a and 9c, adj. $r^2 = 0.51$ vs. 0.73); there is relatively little improvement in the regression parameters between MBT'_{5Me} and MAAT in tropical lakes (Figures 9d and 9f, adj.

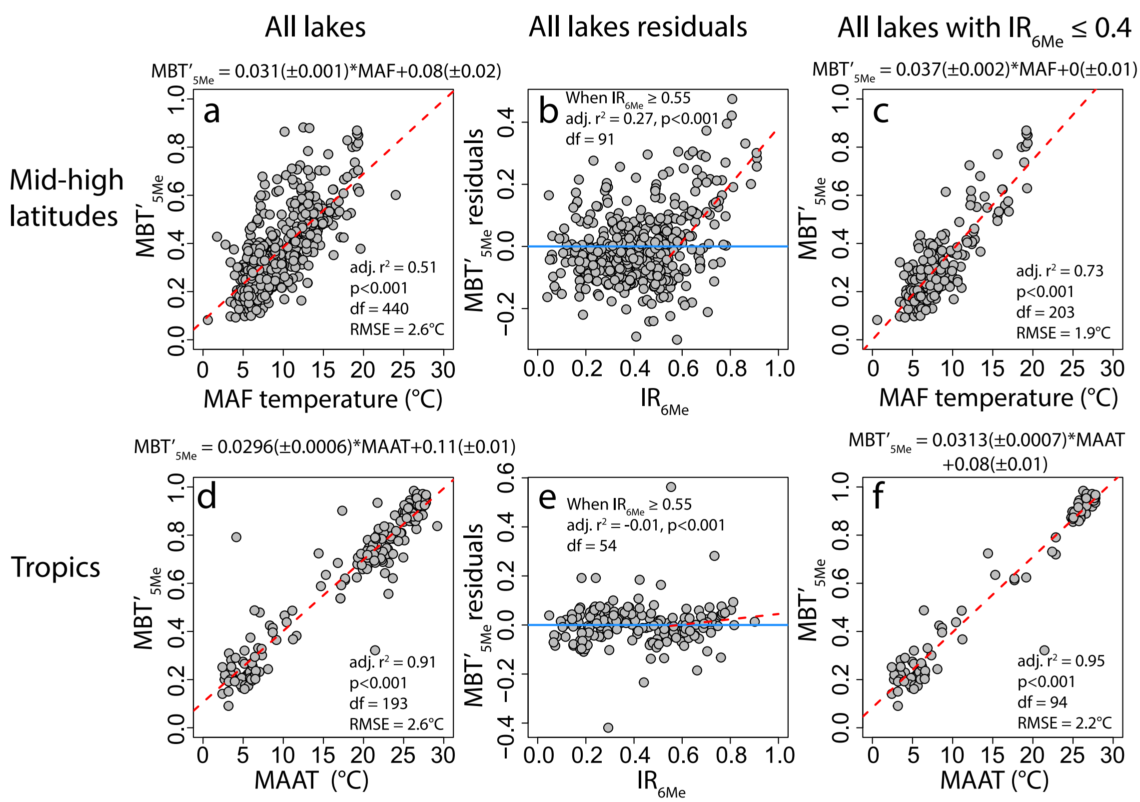

Figure 9. MBT'_{5Me} temperature calibrations for the mid to high latitudes and tropics are improved by removing samples with high IR_{6Me}. (a) Regression between months above freezing air temperature and MBT'_{5Me} in all middle and high latitude lakes. (b) MBT'_{5Me} residuals from the regression in (a) as a function of IR_{6Me}. Red dashed line and regression statistics show the fit between IR_{6Me} and MBT'_{5Me} residuals in samples with $IR_{6Me} \geq 0.55$. (c) Regression between months above freezing air temperature and MBT'_{5Me} in middle and high latitude lakes with $IR_{6Me} \leq 0.4$. (d) Regression between mean annual air temperature and MBT'_{5Me} in all tropical lakes. (e) MBT'_{5Me} residuals from the regression in (d) as a function of IR_{6Me}. Red dashed line and regression statistics show the fit between IR_{6Me} and MBT'_{5Me} residuals in samples with $IR_{6Me} \geq 0.55$. (f) Regression between mean annual air temperature and MBT'_{5Me} in tropical lakes with $IR_{6Me} \leq 0.4$.

$r^2 = 0.91$ vs. 0.96). We also note a weak regression between MBT'_{5Me} and MAF temperature in middle and high latitude lakes with $IR_{6Me} \geq 0.55$ (Figure S16a in Supporting Information S1, adj. $r^2 = 0.09$) but a stronger regression between MBT'_{5Me} and MAAT in tropical lakes with $IR_{6Me} \geq 0.55$ (Figure S16 in Supporting Information S1, adj. $r^2 = 0.45$).

Analysis of the regression residuals shows that exclusion of high IR_{6Me} samples improves the relationship in middle and high latitude lakes but has little effect on the tropical lakes data. The distribution of MBT'_{5Me} in the tropical lake data is somewhat bimodal, which may impact our ability to explore the effects of IR_{6Me}-binning (Figure 9d). However, we note the apparent lack of change in the regression parameters in the relationship between MBT'_{5Me} and MAAT in tropical lakes binned by IR_{6Me} where data density is high (Figures 6c and 6d). We also observed that eliminating lakes with an $IR_{6Me} > 0.4$ from the tropical lake calibration data set removed many samples with small MBT'_{5Me} residuals (Figures 9c–9f). Similarly, we note that middle and high latitude lakes samples with a higher IR_{6Me} tend to have a larger MBT'_{5Me} residual (Figure 9b), while there is only a very slight trend in the residuals from tropical lakes (Figure 9e). We also observed minimal difference in the statistical power of regressing global lake MBT'_{5Me} to MAF in samples from all lakes with $IR_{6Me} \leq 0.4$ compared to only filtering middle and high latitude lakes by IR_{6Me} (Figures 10b vs. 10c).

4. Discussion

4.1. IR_{6Me} as an Indicator of Non-Thermal Influences on MBT'_{5Me} in Lakes

The data suggest IR_{6Me} can detect non-thermal influences on MBT'_{5Me} in middle and high latitude lakes but not tropical lakes (see Section 3.2), but the mechanism(s) causing IR_{6Me} variations and the apparent difference in lakes at different latitudes are unclear. A simple explanation for the differences between the middle to high

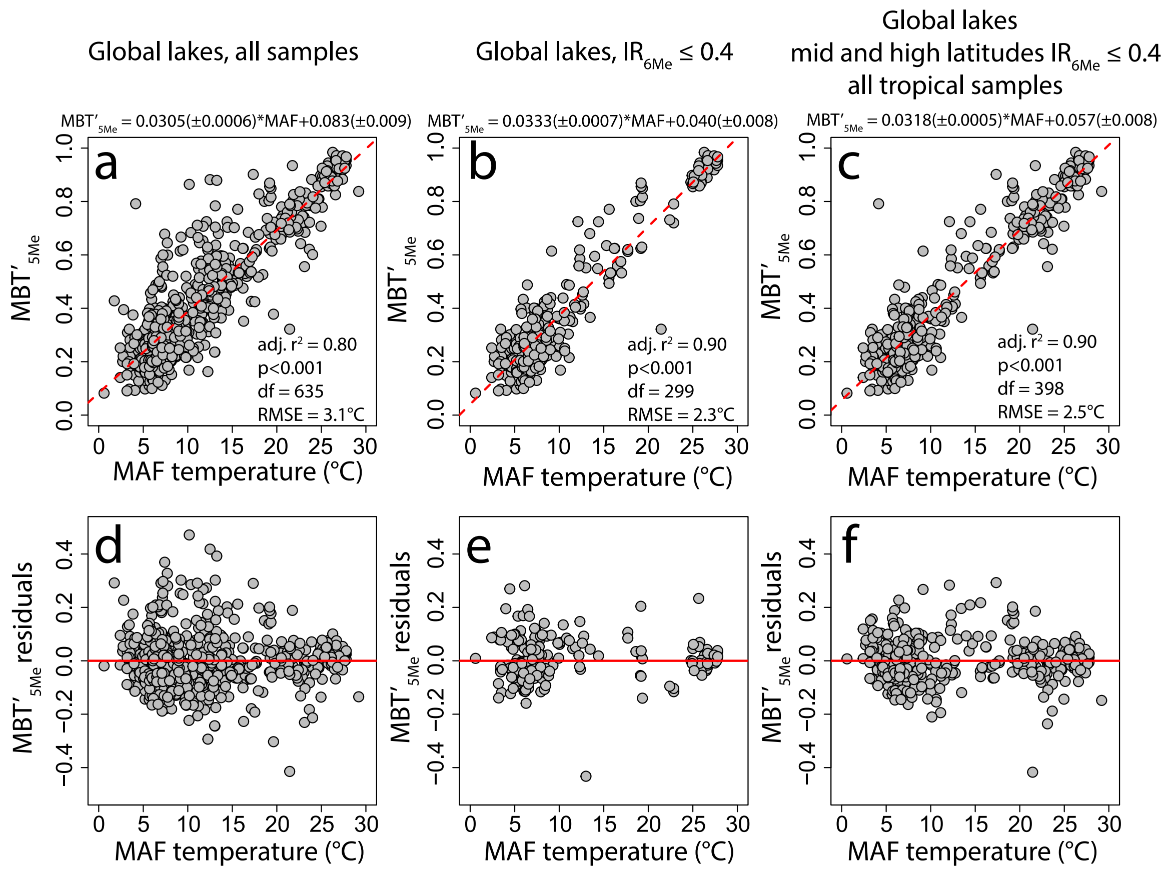

Figure 10. Regressions of MBT'_{5Me} to the global lacustrine surface sediment data set. (a) Regression of MBT'_{5Me} to MAF in all globally distributed lake surface sediment samples. (b) Regression of MBT'_{5Me} to MAF globally distributed in lake surface sediment samples with $IR_{6Me} \leq 0.4$. (c) Regression of MBT'_{5Me} to MAF globally distributed in lake surface sediment samples with $IR_{6Me} \leq 0.4$ used as a filter only for middle and high latitude samples. All tropical lake samples are included regardless of IR_{6Me}. (d) MBT'_{5Me} residuals of the regression shown in (a). (e) MBT'_{5Me} residuals of the regression shown in (b). (f) MBT'_{5Me} residuals of the regression shown in (c). Note that MAF temperature in the tropics is equivalent to MAAT.

latitude and tropical lakes data sets is the bimodal distribution of MAAT sampled by the tropical lake data set. Given the nature of how tropical lakes are formed (Löffler, 1964), samples with temperatures from 10 to 20°C are scarce (e.g., Figures 9d–9f), which is the range of temperatures previously suggested to be most susceptible to IR_{6Me}-related changes in MBT'_{5Me} (Wang et al., 2024). Recently, Wang et al. (2024) observed a systematic change in MBT'_{5Me}-temperature regression slope and intercept across samples grouped by IR_{6Me} and argued for a link between MBT'_{5Me} and the 6-methyl brGDGTs due to the production of tetramethylated brGDGTs by the bacteria responsible for 6-methyl brGDGT production (Wang et al., 2024). The hypothesis that 5-methyl and 6-methyl brGDGTs are synthesized by different organisms is supported by cultured bacteria exclusively producing 5-methyl brGDGTs (Chen et al., 2022; Halamka et al., 2023) and 16S rRNA sequencing of lacustrine suspended particulate matter (van Bree et al., 2020), perhaps suggesting the apparent differences between the middle to high latitude and tropical data sets is due to the range of MAATs sampled by the tropical data relative to the temperature-dependent differences in brGDGT methylation between bacterial communities (Wang et al., 2024). However, it is unlikely that generating tropical lake surface sediment data to test this hypothesis will be straightforward since most montane tropical lakes are at high elevations with MAAT below ∼10°C (cf. Löffler, 1964).

The improved MBT'_{5Me}-temperature calibration on low IR_{6Me} samples (Figure 8) is consistent with previous observations in soil MBT'_{5Me}-temperature calibration studies that linked high IR_{6Me} values to poor model performance and high pH (Dang, Xue, et al., 2016; Dang, Yang, et al., 2016; Naafs, Gallego-Sala, et al., 2017). Perhaps therefore, high lake water pH may be linked to the coincidence of high IR_{6Me} values and MBT'_{5Me} residuals.

Other studies have shown a correlation with higher abundances of 5-methyl and 6-methyl brGDGTs and lower dissolved O_2 in lakes (Weber et al., 2018; Wu et al., 2021). A microcosm incubation experiment demonstrated a doubling of brGDGT concentrations under low O_2 conditions as compared to oxic conditions (Martínez-Sosa & Tierney, 2019), perhaps suggesting that even brief periods of low O_2 in lakes could substantially change the brGDGT distribution integrated into sediments. Some data suggest that oxic conditions result in higher MBT'_{5Me} values when temperature is held constant (Chen et al., 2022), but this is not consistent across experiments (cf. Chen et al., 2022; Halamka et al., 2023). It is also notable that we observed large variations in IR_{6Me} in Lake Baikal surface sediments despite the lack of deep water hypoxic or anoxic zones within the lake (Hohmann et al., 1997; Prokopenko & Williams, 2004; Weiss et al., 1991) (Figure 4a), suggesting that the relationships between brGDGT isomerization and dissolved O_2 observed in some lakes (e.g., Weber et al., 2018; Wu et al., 2021) are not universal.

Lake water salinity has also been linked to changes in brGDGT isomerization (Kou et al., 2022; Wang et al., 2021), leading to the hypothesis that IR_{6Me} can be used to quantitatively account for salinity-driven changes in MBT'_{5Me} in lakes (Wang et al., 2021). However, multivariate regression of MBT'_{5Me} and IR_{6Me} to MAF temperature in middle to high latitude lakes did not attribute statistical significance to the IR_{6Me} term and yields an almost identical correlation coefficient as the regression between MBT'_{5Me} and temperature alone (Figure S17 in Supporting Information S1). The relative abundances of the 7-methyl brGDGTs used in the correction proposed by Wang et al. (2021) are not available in the global data set. Furthermore, Lake Baikal is a freshwater lake with low salinity between 94.5 and 95.5 mg/kg (Shimaraev et al., 2006) and substantial surficial sediment IR_{6Me} variation (Figure 4a). Again, the observations suggest that although salinity can be an important driver of IR_{6Me} variability in some lakes, it is not a universal mechanism.

MBT'_{5Me} and IR_{6Me} may also respond to the relative input of soil-derived brGDGTs to sediments in lakes. MBT'_{5Me} tends to be lower in lake sediments compared to soils both in the globally distributed lakes and soils data sets and in paired lake sediments and catchment soils (Figures S18a and S18c in Supporting Information S1). The apparent "warm bias" in soil brGDGTs (compared to lake sediments) could explain the systematic shift in regression intercept toward higher values that we observe when regressing mid and high latitude lake MBT'_{5Me} to MAF temperatures binned by IR_{6Me} (Figure 6a). However, while IR_{6Me} in lake sediments is sometimes lower than in soils on a broad scale (Figure S18b in Supporting Information S1), there is still substantial overlap between the lakes and soils in the global data set (Figure S18b in Supporting Information S1). Furthermore, there is no significant difference in IR_{6Me} in the paired lake and catchment soils data (Figure S18d in Supporting Information S1), suggesting IR_{6Me} is not an accurate metric for inferring a soil source of 6-methyl brGDGTs to lake sediments.

In summary, there is no common environmental parameter shared between the lakes with $IR_{6Me} > 0.4$ that explains the non-thermal effects on the MBT'_{5Me} index. Lakes with high IR_{6Me} are found in China, southern Russia, Central Europe, the continental United States, Alaska, Canada, and the Southern Cone of South America (Figures S11b and S11c in Supporting Information S1). While many lakes with high IR_{6Me} samples are alkaline (e.g., Dang et al., 2018; Martínez-Sosa et al., 2021) and/or saline (e.g., Wang et al., 2021), others are not (e.g., Bauersachs et al., 2024; Weber et al., 2018). Samples from both deep (>100 m) and shallow (~30 cm) lakes have high IR_{6Me} (Bauersachs et al., 2024; Otiniano et al., 2023; Weber et al., 2018), as do samples from both oxygenated and hypoxic lakes (Wu et al., 2021). Given the diversity of lakes with high IR_{6Me}, we speculate that brGDGT isomerization may be related to multiple environmental factors (e.g., pH, salinity, O_2, brGDGT source) rather than any single variable. Regardless of the cause, lake sediment samples with high IR_{6Me} have a different and poorer relationship between MBT'_{5Me} and temperature. Therefore, screening samples based on IR_{6Me} is a useful approach to identify samples where non-thermal effects are likely, ultimately improving paleotemperature reconstructions.

4.2. Insights Into IR_{6Me} and brGDGT Temperature Estimates From the Lake Baikal Record

Our downcore samples from Lake Baikal demonstrate how IR_{6Me} can be used to identify shifts in brGDGT distributions that impact temperature estimates (Figures 2 and 3). Both the average IR_{6Me} and CBT′ values and the pattern of IR_{6Me} and CBT′ variations between the Last Glacial Maximum and Holocene are the opposite of the pattern in the 250–50 Ka section of the cores (Figure 2b), perhaps suggesting a change in the bacterial communities producing brGDGTs in Lake Baikal. Our results from core VER 92/2-GC24 demonstrate that elevated

IR_{6Me} values of the Lake Baikal GDGTs during the last glacial are observed not only at the distant hemipelagic sites 333 and 340 but also in the pro-deltaic depositional settings where sediment accumulation rates are 4 times higher (Figure 1 and Figure S5 in Supporting Information S1). Thus, deposition of GDGTs with elevated IR_{6Me} during the last glacial is a basin-wide phenomenon in Lake Baikal. Yet, a puzzling aspect of the Lake Baikal brGDGT data set is the absence of a clear event in the lake's geologic history that might have triggered a change in water chemistry or brGDGT provenance changes that are typically used to explain shifts in brGDGT distributions (e.g., Acharya et al., 2023; Parish et al., 2023) (Figure 2). For example, there are no obvious changes in sedimentology (Peck et al., 1994) or lake level (Colman, 1998) between these intervals that would correspond to an increase in lake water pH, salinity, or oxygenation.

Nonetheless, it is in fact possible in the Baikal record to obtain the GDGT-based LGM temperature estimates consistent with both local stratigraphy and the reconstructed values of prior Pleistocene glacials when reconstructing paleotemperature solely from samples with $IR_{6Me} \leq 0.4$ (see also Section 4.3). Principal components analysis of the Lake Baikal data set supports using IR_{6Me} to identify the subset of samples that are suitable for paleotemperature reconstruction (Figure 11). PC1 explains 62.6% of the variance and is strongly correlated with IR_{6Me}, CBT′, MBT'_{5Me}, and temperatures reconstructed with the full set and mixing model methods (Figures 11a–11d). The data suggest that PC1 captures a process or processes that drove changes in brGDGT isomerization and cyclization at Lake Baikal and, in part, methylation (Figure 11b). PC2 explains 13.8% of the variance and is moderately correlated to MBT'_{5Me} and reconstructed temperatures across all methods (Figure 11b), suggesting that PC2 captures changes related to temperature variations within the Lake Baikal brGDGT data set. Notably, we found that MBT'_{5Me} is more strongly correlated to PC2 when grouping samples by IR_{6Me}, especially within the $IR_{6Me} \leq 0.4$ and $IR_{6Me} \geq 0.55$ groups (Figure 11f). We also observed a shift in the intercept and shallowing of the slope of the best fit lines between PC2 and MBT'_{5ME} between groups as expected from our analysis of the global data set (Figures 6a and 6b vs. 11f).

Curiously, despite the poor correlation between MBT'_{5Me} and MAF temperature in middle to high latitude lake surface sediments with $IR_{6Me} \geq 0.55$ (Figure S15a in Supporting Information S1), in Lake Baikal PC2 is correlated to MBT'_{5Me} in samples with $IR_{6Me} \geq 0.55$ ($r^2 = 0.63$, $p < 0.001$). This observation and the significant differences in reconstructed MAF temperatures between glacial clays and interglacial diatom oozes (Figure S8 in Supporting Information S1) perhaps suggest that it is possible for site-specific calibrations to extract paleotemperatures from some lakes in the middle and high latitudes with high IR_{6Me}.

We suggest that the correlation between Lake Baikal IR_{6Me} and sedimentary brGDGT concentrations reflects mixing between IR_{6Me} endmembers (Figure 4a). The variable expression of this mixing could result from large changes in the contributions from either source, perhaps supporting a scheme like that proposed by Wang et al. (2024) in which brGDGT inputs to sediments come from multiple bacterial groups. The anomalously warm temperatures generated from the Wang et al. (2024) mixing model method may result from different endmember values or an insufficient number of endmembers for Lake Baikal (Figures 3g and 3h).

4.3. Reconstructing Temperatures From Complex Lacustrine brGDGT Samples

Our observations support restricting paleotemperature reconstructions at Lake Baikal to samples with $IR_{6Me} \leq 0.4$, at least until a more suitable method for extracting paleotemperatures from samples with high IR_{6Me} can be developed. This approach reconstructs a most recent (2.9 Ka) MAF temperature estimate of 9.3 ± 2.3°C (equation in Figure 10b), in good agreement with 1998–2016 average summer water temperature (8–11°C; Figure 1, site 333). Reconstructed Holocene MAF temperatures from samples with $IR_{6Me} \leq 0.4$ are broadly in agreement with those of MIS 5 and 7 (Figure 12). Likewise, the reconstructed Last Glacial period MAF temperature from VER92/2-GC24 is in agreement with our estimates for MIS 4 and 6 from the Academician Ridge piston core composite (Figure 12). This result conforms with our expectations based upon both global climate trends (Lisiecki & Raymo, 2005) and previous qualitative reconstructions of climate at Lake Baikal over this interval (BDP-99 Members, 2005; Colman et al., 1995; Karabanov et al., 2000; Khursevich et al., 2001; Peck et al., 1994; Prokopenko et al., 2006; P. Tarasov et al., 2007; P. E. Tarasov et al., 2005), which are represented here by our dry bulk density data (Figure 12). The example of the GC-24 20-Ka sample shows that when not associated with high IR_{6Me}, the MBT'_{5Me} temperature index adequately captures glacial-interglacial temperature variations in Lake Baikal.

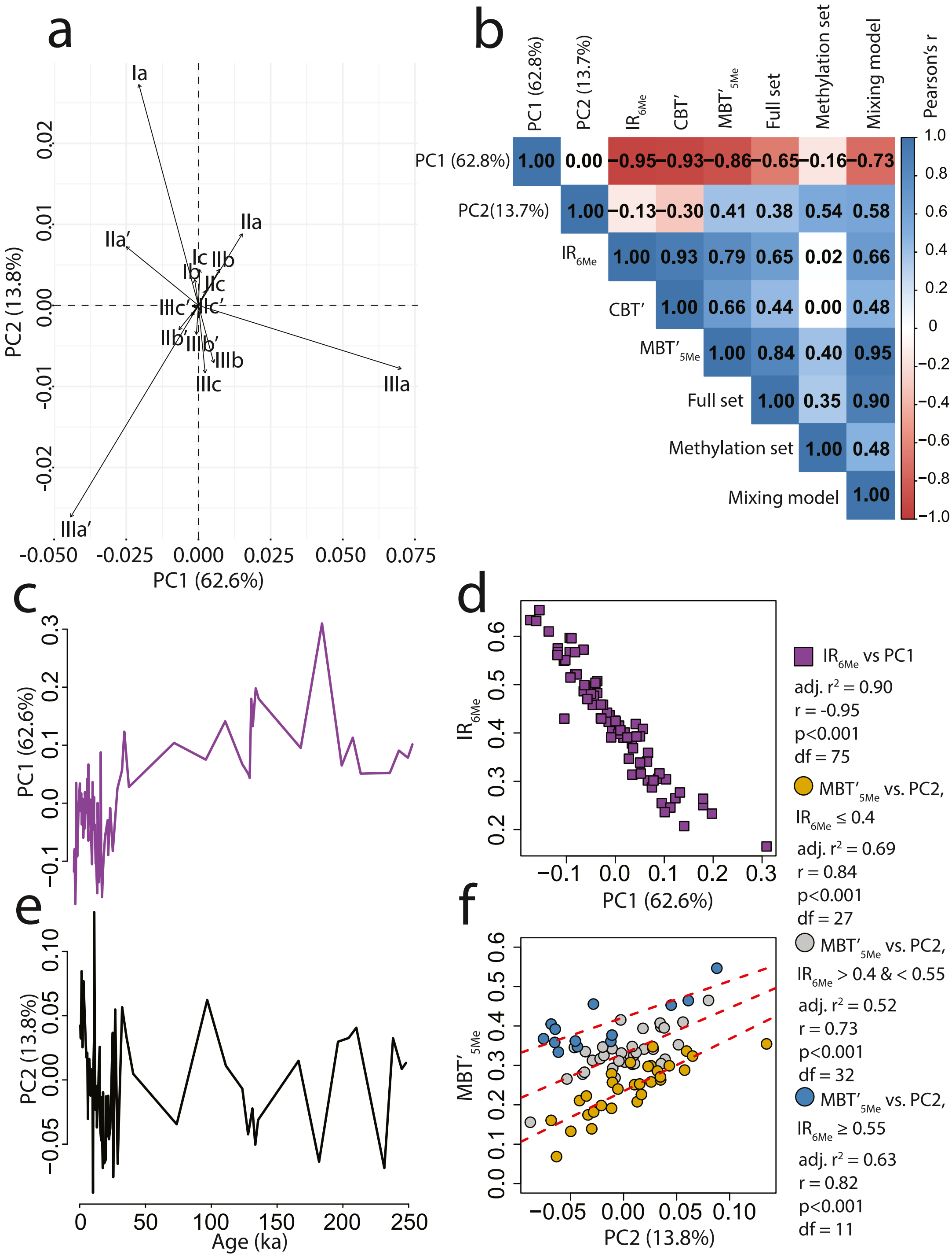

Figure 11. Principal component analysis of the Lake Baikal brGDGT downcore data set. (a) Loadings of individual brGDGTs on PC1 and PC2. (b) Correlation matrix showing Pearson's *r* between PC1, PC2, brGDGT indices, and temperatures reconstructed with the methods of Raberg et al. (2021) (full set and methylation set) and Wang et al. (2024) (mixing model). (c) Timeseries of PC1. (d) Correlation between IR_{6Me} and PC1. (e) Timeseries of PC2. (f) Correlation between MBT'_{5Me} and PC2. Samples in (f) are grouped by IR_{6Me}. Red dashed lines are the lines of best fit for each sample group.

These observations further support the idea that filtering the GDGT-based temperature estimates by their associated IR_{6Me} values is likely to greatly improve paleotemperature reconstructions both regionally and globally. We argue that applying an MBT'_{5Me}-based temperature calibration based on lacustrine surface sediment samples

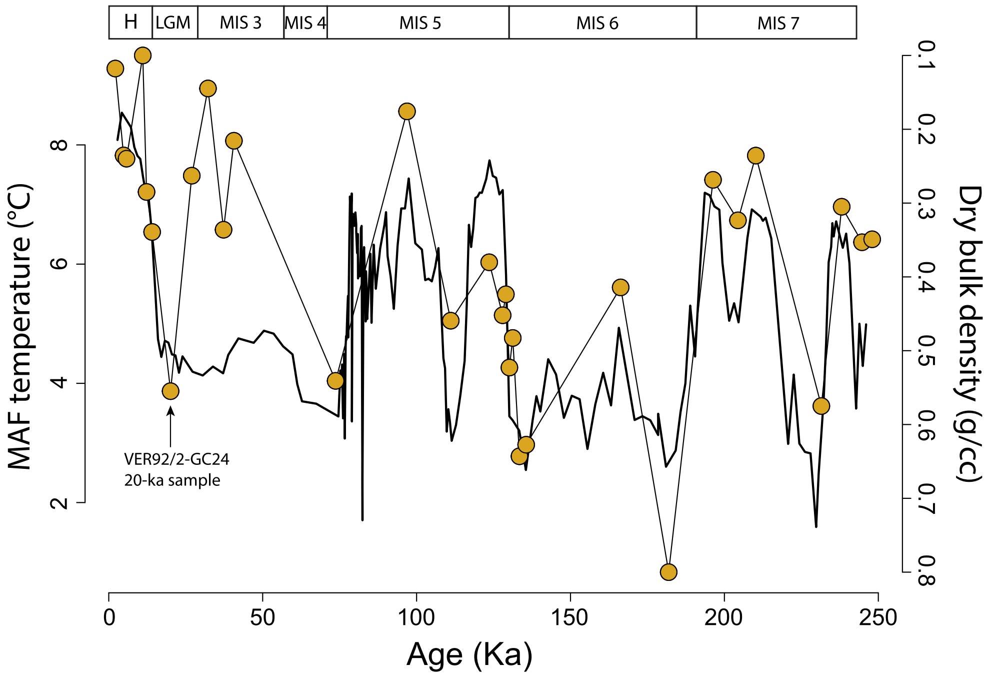

Figure 12. The IR_{6Me}-filtered Lake Baikal brGDGT temperature record. H = Holocene. LGM = Last Glacial Maximum. MIS = Marine Isotope Stage. MIS boundaries are defined by Lisiecki and Raymo (2005).

with $IR_{6Me} \leq 0.4$ to deeper sediment samples, also with $IR_{6Me} \leq 0.4$, restricts lacustrine paleotemperature records to sample sets similar to the population of surface sediment samples with the strongest calibrated relationship to MAF temperature (Figure 10). This view is supported by our analysis suggesting that removing samples with $IR_{6Me} > 0.4$ from the Lake Baikal paleotemperature record limits temperature reconstruction to a population of samples with brGDGTs that respond to temperature change similarly (Figure 11).

The strengthening of the middle and high latitude lake MBT'_{5Me}-temperature calibration suggests that our approach to reconstructing paleotemperatures at Lake Baikal may prove useful elsewhere (Figure 9). We recommend screening brGDGT samples by their IR_{6Me} as a first-order method to limit lacustrine paleotemperature reconstructions to samples with a similar temperature response, albeit at the expense of possibly excluding many brGDGT measurements from the paleotemperature reconstruction, as was the case at Lake Baikal (Figure 2 vs. 12). A more precise understanding of the cause(s) of IR_{6Me} variability is necessary to better predict which lakes or coring sites are most likely to yield brGDGT distributions useful for paleotemperature reconstruction.

4.4. Role of Seasonality in the MBT'_{5Me}- Temperature Calibration

The correct seasonal weighting of temperatures for regression of MBT'_{5Me} in mid and high latitude lakes remains an ongoing challenge. While IR_{6Me} substantially improves MBT'_{5Me}- temperature regressions, it does not address how seasonality in brGDGT production or differences in air versus lake water temperatures impact the calibration (Zhao et al., 2023). Limited studies of suspended particulate matter in lakes suggest that the majority of brGDGTs produced in lakes are synthesized during seasonal mixing, though some proportion of brGDGTs are also produced during other seasons (Loomis et al., 2014; Miller et al., 2018; Zhao et al., 2021). The large temperature seasonality of the middle and high latitudes imparts a seasonal mixing regime (often dimictic or cold monomictic) (Woolway & Merchant, 2019) that could bias brGDGT production to specific seasons and, therefore, temperatures. Furthermore, the relationship between air and lake water temperature becomes more complicated with large seasonal temperature variations; rapidly changing lake energy budgets determine the seasonal progression of lake water temperature, and cold temperatures are truncated due to the freezing point of water (MacIntyre & Melack, 2010). The average months above freezing air temperature used here seek to account for lower brGDGT production during ice-covered periods and to approximate lake water temperature during ice-free periods. However, the progression of lake temperature and brGDGT production during the ice-free period will be

10.1029/2024GC012069

modulated by lake volume, basin morphology, overturning dynamics, and epilimnion volume (Toffolon et al., 2014), factors imperfectly captured in the average months above freezing temperature. Therefore, some of the scatter in the calibration may simply be the consequence of lake-to-lake differences in such factors.

As anticipated from the seasonality of the temperatures used for the regression analysis, there is a difference in the slope of the temperature calibration equations between the middle and high latitude lakes and tropical lakes (Figure 9) as also found by Zhao et al. (2023). Furthermore, while the global MBT'_{5Me} temperature regression statistics are improved by restricting the calibration data set to samples with $IR_{6Me} \leq 0.4$ (Figures 10a–10c), the slope of the best fit line still falls between those of the middle to high latitude and tropical lake regression equations (Figures 10a and 10b) and a trend in the MBT'_{5Me} residuals between 0 and 10°C persists in both the global calibrations regardless of how the data are grouped (Figures 10d–10f) and in the middle and high latitude MBT'_{5Me} temperature regression for samples with $IR_{6Me} \leq 0.4$ (Figure S19b in Supporting Information S1).

The different slopes of the MBT'_{5Me}-temperature regressions in tropical and extratropical settings occur despite the expectation that similar biochemical or ecological processes are driving the response of MBT'_{5Me} to temperature (Raberg, Flores, et al., 2022; Raberg, Miller, et al., 2022). Calibration temperatures of tropical and extratropical lake overlap at low MBT'_{5Me} values but diverge at high MBT'_{5Me} (e.g., Figures 9a vs. 9d). Therefore, the different slopes are largely the consequence of data points from higher MBT'_{5Me} (warmer) lakes. Imperfect estimation of the correct temperature for these lakes is a likely source of this discrepancy (Zhao et al., 2023). For example, cool but above-freezing winter temperatures in these lakes will decrease the average air temperature used in the calibration, while the subzero air temperatures of lakes in colder regions will be excluded from the calibration. If brGDGT production is more heavily weighted to spring-summer-fall, the calibration temperatures of these "warmer" extratropical lakes will systematically underestimate the brGDGT production temperature (as observed in the calibration, Figures 9 and 10). The discrepancy between the tropical and extratropical MBT'_{5Me}-temperature calibration slopes suggests that further improvements in the calibration are needed to better estimate the temperatures at the time brGDGTs were produced and exported to sediments in extratropical lakes.

5. Conclusions

We presented a new brGDGT record from Lake Baikal, Russia, characterized by anomalously warm reconstructed paleotemperatures over the last 50 Ka compared to the deeper sediments. These unusually warm reconstructed temperatures were systematically accompanied by high IR_{6Me} and CBT' values. We built upon previous work investigating the link between brGDGT isomerization and the MBT'_{5Me} index (Bauersachs et al., 2024; Naafs, Gallego-Sala, et al., 2017; Wang et al., 2024) by demonstrating that MBT'_{5Me}-temperature calibration residuals are correlated to IR_{6Me} in middle and high latitude lakes. We did not observe similar IR_{6Me}-related trends in the tropical lakes data set. Restricting the middle and high latitude lakes surface sediment calibration data set to samples with $IR_{6Me} \leq 0.4$ substantially strengthens the correlation between MBT'_{5Me} and months above freezing air temperature. Likewise, restricting the Lake Baikal downcore data set to samples with $IR_{6Me} \leq 0.4$ appears to eliminate the non-thermal overprint on the paleotemperature record, at the expense of rejecting samples from the final paleotemperature timeseries. Our findings point toward brGDGT isomerization as an important aspect of brGDGT distributions that must be considered when assessing brGDGT methylation as a temperature proxy in lacustrine sediments.

Inclusion in Global Research Statement

We thank the Baikal Drilling Project and its many members for collection, archiving, and access to sample materials.

Conflict of Interest

The authors declare no conflicts of interest relevant to this study.

Data Availability Statement

All data associated with this manuscript are available as.xlxs files in Supporting Information S1 and are electronically archived at PANGAEA (Novak et al., 2025).

10.1029/2024GC012069

Acknowledgments

The authors thank Dr. Gerard Otiniano, Dr. Jonathan Raberg, and an anonymous reviewer for their comments on the manuscript, which substantially improved the work. The authors thank Dr. Marcelo R. Alexandre for assistance analyzing GDGTs at Brown University. This work was supported by National Science Foundation funding to J.B.N. and P.J.P. (NSF NNA 22-02918), Geological Society of America Continental Drilling Science Division Graduate Student Grant 13282-21 to J.B.N., and Sigma Xi Grants in Aid of Research G20211001-101 to J.B.N. The ARCS scholarship supported J.B.N. Lake Baikal sediments discussed in this study were collected by the Baikal Drilling Project and Roberts et al. (2018) and Swann et al. (2018), supported by Natural Environment Research Council grants NE/J00829X/1, NE/J010227/1, and NE/J007765/1 to G.E.A.S. Baikal Drilling Project materials were provided by the University of Rhode Island Marine Geological Samples Laboratory, supported by NSF OCE 2116199, generously shared with us by Dr. John King and curated by Dr. Rebecca Robinson. BAIK sample materials were provided by Dr. George E. A. Swann.

References

Acharya, S., Zech, R., Strobel, P., Bliedtner, M., Prochnow, M., & De Jonge, C. (2023). Environmental controls on the distribution of GDGT molecules in Lake Höglwörth, Southern Germany. *Organic Geochemistry*, *186*, 104689. https://doi.org/10.1016/j.orggeochem.2023.104689

Auderset, A., Schmitt, M., & Martínez-García, A. (2020). Simultaneous extraction and chromatographic separation of n-alkanes and alkenones from glycerol dialkyl glycerol tetraethers via selective Accelerated Solvent Extraction. *Organic Geochemistry*, *143*, 103979. https://doi.org/10.1016/j.orggeochem.2020.103979

Bauersachs, T., Schubert, C. J., Mayr, C., Gilli, A., & Schwark, L. (2024). Branched GDGT-based temperature calibrations from Central European lakes. *Science of the Total Environment*, *906*, 167724. https://doi.org/10.1016/j.scitotenv.2023.167724

Baxter, A. J., Hopmans, E. C., Russell, J. M., & Sinninghe Damsté, J. S. (2019). Bacterial GMGTs in East African lake sediments: Their potential as palaeotemperature indicators. *Geochimica et Cosmochimica Acta*, *259*, 155–169. https://doi.org/10.1016/j.gca.2019.05.039

BDP-99 Members. (2005). A new Quaternary record of regional tectonic, sedimentation and paleoclimate changes from drill core BDP-99 at Posolskaya Bank, Lake Baikal. *Quaternary International*, *136*(1 SPEC. ISS.), 105–121. https://doi.org/10.1016/j.quaint.2004.11.012

Braconnot, P., Harrison, S. P., Kageyama, M., Bartlein, P. J., Masson-Delmotte, V., Abe-Ouchi, A., et al. (2012). Evaluation of climate models using palaeoclimatic data. *Nature Climate Change*, *2*(6), 417–424. https://doi.org/10.1038/nclimate1456

Cao, J., Rao, Z., Shi, F., & Jia, G. (2020). Ice formation on lake surfaces in winter causes warm-season bias of lacustrine brGDGT temperature estimates. *Biogeosciences*, *17*(9), 2521–2536. https://doi.org/10.5194/bg-17-2521-2020

Carrea, L., & Merchant, C. J. (2019). *GloboLakes: Lake surface water temperature (LSWT) v4. 0 (1995–2016)* (Vol. 10, p. 29). Centre for Environmental Data Analysis.

Carter, S. J., & Colman, S. M. (1994). Biogenic Silica in Lake Baikal Sediments: Results From 1990–1992 American Cores. *Journal of Great Lakes Research*, *20*(4), 751–760. https://doi.org/10.1016/S0380-1330(94)71192-8

Chen, Y., Zheng, F., Yang, H., Yang, W., Wu, R., Liu, X., et al. (2022). The production of diverse brGDGTs by an Acidobacterium providing a physiological basis for paleoclimate proxies. *Geochimica et Cosmochimica Acta*, *337*, 155–165. https://doi.org/10.1016/j.gca.2022.08.033

Cluett, A. A., Thomas, E. K., McKay, N. P., Cowling, O. C., Castañeda, I. S., & Morrill, C. (2023). Lake Dynamics Modulate the Air Temperature Variability Recorded by Sedimentary Aquatic Biomarkers: A Holocene Case Study From Western Greenland. *Journal of Geophysical Research: Biogeosciences*, *128*(7). https://doi.org/10.1029/2022JG007106

Colman, S. M. (1998). Water-level changes in Lake Baikal, Siberia: Tectonism versus climate. *Geology*, *26*(6), 531–534. https://doi.org/10.1130/0091-7613(1998)026<0531:wlcilb>2.3.co;2

Colman, S. M., Jones, G. A., Rubin, M., King, J. W., Peck, J. A., & Orem, W. H. (1996). AMS radiocarbon analyses from Lake Baikal, Siberia: Challenges of dating sediments from a large, oligotrophic lake. *Quaternary Science Reviews*, *15*(7), 669–684. https://doi.org/10.1016/0277-3791(96)00027-3

Colman, S. M., Peck, J. A., Karabanov, E. B., Carter, S. J., Bradbury, J. P., King, J. W., & Williams, D. F. (1995). Continental climate response to orbital forcing from biogenic silica records in Lake Baikal. *Nature*, *378*(6559), 703–706. https://doi.org/10.1038/378769a0

Damsté, J. S. S., Hopmans, E. C., Pancost, R. D., Schouten, S., & Geenevasen, J. A. J. (2000). Newly discovered non-isoprenoid glycerol dialkyl glycerol tetraether lipids in sediments. *Chemical Communications*(17), 1683–1684. https://doi.org/10.1039/b004517i

Dang, X., Ding, W., Yang, H., Pancost, R. D., Naafs, B. D. A., Xue, J., et al. (2018). Different temperature dependence of the bacterial brGDGT isomers in 35 Chinese lake sediments compared to that in soils. *Organic Geochemistry*, *119*, 72–79. https://doi.org/10.1016/j.orggeochem.2018.02.008

Dang, X., Yang, H., Naafs, B. D. A., Pancost, R. D., & Xie, S. (2016). Evidence of moisture control on the methylation of branched glycerol dialkyl glycerol tetraethers in semi-arid and arid soils. *Geochimica et Cosmochimica Acta*, *189*, 24–36. https://doi.org/10.1016/j.gca.2016.06.004

Dang, X. Y., Xue, J., Yang, H., & Xie, S. (2016). Environmental impacts on the distribution of microbial tetraether lipids in Chinese lakes with contrasting pH: Implications for lacustrine paleoenvironmental reconstructions. *Science China Earth Sciences*, *59*(5), 939–950. https://doi.org/10.1007/s11430-015-5234-z

Dearing Crampton-Flood, E., Tierney, J. E., Peterse, F., Kirkels, F. M. S. A., & Sinninghe Damsté, J. S. (2020). BayMBT: A Bayesian calibration model for branched glycerol dialkyl glycerol tetraethers in soils and peats. *Geochimica et Cosmochimica Acta*, *268*, 142–159. https://doi.org/10.1016/j.gca.2019.09.043

De Jonge, C., Hopmans, E. C., Stadnitskaia, A., Rijpstra, W. I. C., Hofland, R., Tegelaar, E., & Sinninghe Damsté, J. S. (2013). Identification of novel penta- and hexamethylated branched glycerol dialkyl glycerol tetraethers in peat using HPLC–MS2, GC–MS and GC–SMB-MS. *Organic Geochemistry*, *54*, 78–82. https://doi.org/10.1016/j.orggeochem.2012.10.004

De Jonge, C., Hopmans, E. C., Zell, C. I., Kim, J. H., Schouten, S., & Sinninghe Damsté, J. S. (2014). Occurrence and abundance of 6-methyl branched glycerol dialkyl glycerol tetraethers in soils: Implications for palaeoclimate reconstruction. *Geochimica et Cosmochimica Acta*, *141*, 97–112. https://doi.org/10.1016/j.gca.2014.06.013

De Jonge, C., Stadnitskaia, A., Fedotov, A., & Sinninghe Damsté, J. S. (2015). Impact of riverine suspended particulate matter on the branched glycerol dialkyl glycerol tetraether composition of lakes: The outflow of the Selenga River in Lake Baikal (Russia). *Organic Geochemistry*, *83–84*, 241–252. https://doi.org/10.1016/j.orggeochem.2015.04.004

Ding, S., Xu, Y., Wang, Y., He, Y., Hou, J., Chen, L., & He, J.-S. (2015). Distribution of branched glycerol dialkyl glycerol tetraethers in surface soils of the Qinghai–Tibetan Plateau: Implications of brGDGTs-based proxies in cold and dry regions. *Biogeosciences*, *12*(11), 3141–3151. https://doi.org/10.5194/bg-12-3141-2015

Dugerdil, L., Joannin, S., Peyron, O., Jouffroy-Bapicot, I., Vannière, B., Boldgiv, B., & Ménot, G. (2020). Climate reconstructions based on GDGTs and pollen surface datasets from Mongolia and Siberia: Calibrations and applicability to extremely dry and cold environments. *Biogeosciences Discussions*, 1–35. https://doi.org/10.5194/bg-2019-475

Fick, S. E., & Hijmans, R. J. (2017). WorldClim 2: New 1-km spatial resolution climate surfaces for global land areas. *International Journal of Climatology*, *37*(12), 4302–4315. https://doi.org/10.1002/joc.5086

Halamka, T. A., Raberg, J. H., McFarlin, J. M., Younkin, A. D., Mulligan, C., Liu, X., & Kopf, S. H. (2023). Production of diverse brGDGTs by Acidobacterium *Solibacter usitatus* in response to temperature, pH, and O_2 provides a culturing perspective on brGDGT proxies and biosynthesis. *Geobiology*, *21*(1), 102–118. https://doi.org/10.1111/gbi.12525

Hampton, S. E., Izmest'eva, L. R., Moore, M. V., Katz, S. L., Dennis, B., & Silow, E. A. (2008). Sixty years of environmental change in the world's largest freshwater lake—Lake Baikal, Siberia. *Global Change Biology*, *14*(8), 1947–1958. https://doi.org/10.1111/j.1365-2486.2008.01616.x

Hohmann, R., Kipfer, R., Peeters, F., Piepke, G., Imboden, D. M., & Shimaraev, M. N. (1997). Processes of deep-water renewal in Lake Baikal. *Limnology & Oceanography*, *42*(5), 841–855. https://doi.org/10.4319/lo.1997.42.5.0841

Hopmans, E. C., Schouten, S., Pancost, R. D., van der Meer, M. T. J., & Sinninghe Damste, J. S. (2000). Analysis of intact tetraether lipids in archaeal cell material and sediments by high performance liquid chromatography/atmospheric pressure chemical ionization mass spectrometry. *Rapid Communications in Mass Spectromerty*, *14*(7), 585–589. https://doi.org/10.1002/(sici)1097-0231(20000415)14:7<585::aid-rcm913>3.0.co;2-n

Hopmans, E. C., Schouten, S., & Sinninghe Damsté, J. S. (2016). The effect of improved chromatography on GDGT-based palaeoproxies. *Organic Geochemistry*, *93*, 1–6. https://doi.org/10.1016/j.orggeochem.2015.12.006

Hopmans, E. C., Weijers, J. W. H., Schefuß, E., Herfort, L., Sinninghe Damsté, J. S., & Schouten, S. (2004). A novel proxy for terrestrial organic matter in sediments based on branched and isoprenoid tetraether lipids. *Earth and Planetary Science Letters*, *224*(1–2), 107–116. https://doi.org/10.1016/j.epsl.2004.05.012

Huguet, C., Hopmans, E. C., Febo-Ayala, W., Thompson, D. H., Sinninghe Damsté, J. S., & Schouten, S. (2006). An improved method to determine the absolute abundance of glycerol dibiphytanyl glycerol tetraether lipids. *Organic Geochemistry*, *37*(9), 1036–1041. https://doi.org/10.1016/j.orggeochem.2006.05.008

Inglis, G. N., Farnsworth, A., Collinson, M. E., Carmichael, M. J., Naafs, B. D. A., Lunt, D. J., et al. (2019). Terrestrial environmental change across the onset of the PETM and the associated impact on biomarker proxies: A cautionary tale. *Global and Planetary Change*, *181*, 102991. https://doi.org/10.1016/j.gloplacha.2019.102991

Karabanov, E., Williams, D., Kuzmin, M., Sideleva, V., Khursevich, G., Prokopenko, A., et al. (2004). Ecological collapse of Lake Baikal and Lake Hovsgol ecosystems during the Last Glacial and consequences for aquatic species diversity. *Palaeogeography, Palaeoclimatology, Palaeoecology*, *209*(1–4), 227–243. https://doi.org/10.1016/j.palaeo.2004.02.017

Karabanov, E. B., Prokopenko, A. A., Williams, D. F., & Khursevich, G. K. (2000). Evidence for mid-Eemian cooling in continental climatic record from Lake Baikal. *Journal of Paleolimnology*, *23*.

Khursevich, G. K., Karabanov, E. B., Prokopenko, A. A., Williams, D. F., Kuzmin, M. I., Fedenya, S. A., & Gvozdkov, A. A. (2001). Insolation regime in Siberia as a major factor controlling diatom production in Lake Baikal during the past 800,000 years. *Quaternary International*, *80–81*, 47–58. https://doi.org/10.1016/S1040-6182(01)00018-0

Kielhofer, J. R., Tierney, J. E., Reuther, J. D., Potter, B. A., Holmes, C. E., Lanoë, F. B., et al. (2023). BrGDGT temperature reconstruction from interior Alaska: Assessing 14,000 years of deglacial to Holocene temperature variability and potential effects on early human settlement. *Quaternary Science Reviews*, *303*, 107979. https://doi.org/10.1016/j.quascirev.2023.107979

Kou, Q., Zhu, L., Ju, J., Wang, J., Xu, T., Li, C., & Ma, Q. (2022). Influence of salinity on glycerol dialkyl glycerol tetraether-based indicators in Tibetan Plateau lakes: Implications for paleotemperature and paleosalinity reconstructions. *Palaeogeography, Palaeoclimatology, Palaeoecology*, *601*, 111127. https://doi.org/10.1016/j.palaeo.2022.111127

Kouraev, A. V., Semovski, S. V., Shimaraev, M. N., Mognard, N. M., Legrés, B., & Remy, F. (2007). The ice regime of Lake Baikal from historical and satellite data: Relationship to air temperature, dynamical, and other factors. *Limnology & Oceanography*, *52*(3), 1268–1286. https://doi.org/10.4319/lo.2007.52.3.1268

Lei, Y., Yang, H., Dang, X., Zhao, S., & Xie, S. (2016). Absence of a significant bias towards summer temperature in branched tetraether-based paleothermometer at two soil sites with contrasting temperature seasonality. *Organic Geochemistry*, *94*, 83–94. https://doi.org/10.1016/j.orggeochem.2016.02.003

Li, J., Naafs, B. D. A., Pancost, R. D., Yang, H., Liu, D., & Xie, S. (2017). Distribution of branched tetraether lipids in ponds from Inner Mongolia, NE China: Insight into the source of brGDGTs. *Organic Geochemistry*, *112*, 127–136. https://doi.org/10.1016/j.orggeochem.2017.07.005

Liang, J., Guo, Y., Richter, N., Xie, H., Vachula, R. S., Lupien, R. L., et al. (2022). Calibration and Application of Branched GDGTs to Tibetan Lake Sediments: The Influence of Temperature on the Fall of the Guge Kingdom in Western Tibet, China. *Paleoceanography and Paleoclimatology*, *37*(5). https://doi.org/10.1029/2021PA004393

Lisiecki, L. E., & Raymo, M. E. (2005). A Pliocene-Pleistocene stack of 57 globally distributed benthic $\delta^{18}O$ records. *Paleoceanography*, *20*(1), 1–17. https://doi.org/10.1029/2004PA001071

Löffler, H. (1964). The limnology of tropical high-mountain lakes. *SIL Proceedings, 1922-2010*, *15*(1), 176–193. https://doi.org/10.1080/03680770.1962.11895519

Loomis, S. E., Russell, J. M., Heureux, A. M., D'Andrea, W. J., & Sinninghe Damsté, J. S. (2014). Seasonal variability of branched glycerol dialkyl glycerol tetraethers (brGDGTs) in a temperate lake system. *Geochimica et Cosmochimica Acta*, *144*, 173–187. https://doi.org/10.1016/j.gca.2014.08.027

MacIntyre, S., & Melack, J. M. (2010). Mixing dynamics in lakes across climatic zones. In *Lake ecosystem ecology: A global perspective* (pp. 86–95).

Martínez-Sosa, P., & Tierney, J. E. (2019). Lacustrine brGDGT response to microcosm and mesocosm incubations. *Organic Geochemistry*, *127*, 12–22. https://doi.org/10.1016/j.orggeochem.2018.10.011

Martínez-Sosa, P., Tierney, J. E., Pérez-Angel, L. C., Stefanescu, I. C., Guo, J., Kirkels, F., et al. (2023). Development and Application of the Branched and Isoprenoid GDGT Machine Learning Classification Algorithm (BIGMaC) for Paleoenvironmental Reconstruction. *Paleoceanography and Paleoclimatology*, *38*(7). https://doi.org/10.1029/2023PA004611

Martínez-Sosa, P., Tierney, J. E., Stefanescu, I. C., Dearing Crampton-Flood, E., Shuman, B. N., & Routson, C. (2021). A global Bayesian temperature calibration for lacustrine brGDGTs. *Geochimica et Cosmochimica Acta*, *305*, 87–105. https://doi.org/10.1016/j.gca.2021.04.038

Miller, D. R., Habicht, M. H., Keisling, B. A., Castañeda, I. S., & Bradley, R. S. (2018). A 900-year New England temperature reconstruction from in situ seasonally produced branched glycerol dialkyl glycerol tetraethers (brGDGTs). *Climate of the Past*, *14*(11), 1653–1667. https://doi.org/10.5194/cp-14-1653-2018

Naafs, B. D. A., Gallego-Sala, A. V., Inglis, G. N., & Pancost, R. D. (2017). Refining the global branched glycerol dialkyl glycerol tetraether (brGDGT) soil temperature calibration. *Organic Geochemistry*, *106*, 48–56. https://doi.org/10.1016/j.orggeochem.2017.01.009

Naafs, B. D. A., Inglis, G. N., Zheng, Y., Amesbury, M. J., Biester, H., Bindler, R., et al. (2017). Introducing global peat-specific temperature and pH calibrations based on brGDGT bacterial lipids. *Geochimica et Cosmochimica Acta*, *208*, 285–301. https://doi.org/10.1016/j.gca.2017.01.038

Naafs, B. D. A., Oliveira, A. S. F., & Mulholland, A. J. (2021). Molecular dynamics simulations support the hypothesis that the brGDGT paleothermometer is based on homeoviscous adaptation. *Geochimica et Cosmochimica Acta*, *312*, 44–56. https://doi.org/10.1016/j.gca.2021.07.034

Ning, D., Zhang, E., Shulmeister, J., Chang, J., Sun, W., & Ni, Z. (2019). Holocene mean annual air temperature (MAAT) reconstruction based on branched glycerol dialkyl glycerol tetraethers from Lake Ximenglongtan, southwestern China. *Organic Geochemistry*, *133*, 65–76. https://doi.org/10.1016/j.orggeochem.2019.05.003

Novak, J. B., Russell, J. M., Lindemuth, E., Prokopenko, A. A., Perez-Angel, L., Zhao, B., et al. (2025). Compiled globally-distributed brGDGT data [Dataset bundled publication]. *PANGAEA*. https://doi.pangaea.de/10.1594/PANGAEA.973601

Otiniano, G., Porter, T. J., Buceta, R., Bergman, M. E., & Phillips, M. A. (2023). Climatic and environmentally driven variability in lacustrine brGDGT distributions at local to regional scales in Alaska and northwestern Canada. *Organic Geochemistry*, *181*, 104604. https://doi.org/10.1016/j.orggeochem.2023.104604

Parish, M. C., Du, X., Bijaksana, S., & Russell, J. M. (2023). A brGDGT-based reconstruction of Terrestrial Temperature From the Maritime Continent Spanning the Last Glacial Maximum. *Paleoceanography and Paleoclimatology*, *38*(3). https://doi.org/10.1029/2022PA004501

Pawlowicz, R. (2020). M_Map: A mapping package for MATLAB, version 1.4m. Retrieved from https://www.eoas.ubc.ca/~rich/map.html

Peck, J. A., King, J. W., Colman, S. M., & Kravchinsky, V. A. (1994). A rock-magnetic record from Lake Baikal, Siberia: Evidence for Late Quaternary climate change. *Earth and Planetary Science Letters*, *122*(1–2), 221–238. https://doi.org/10.1016/0012-821X(94)90062-0

Peterse, F., van der Meer, J., Schouten, S., Weijers, J. W. H., Fierer, N., Jackson, R. B., et al. (2012). Revised calibration of the MBT–CBT paleotemperature proxy based on branched tetraether membrane lipids in surface soils. *Geochimica et Cosmochimica Acta*, *96*, 215–229. https://doi.org/10.1016/j.gca.2012.08.011

Petit, C., & Déverchère, J. (2006). Structure and evolution of the Baikal rift: A synthesis. *Geochemistry, Geophysics, Geosystems*, *7*(11). https://doi.org/10.1029/2006GC001265

Powers, L., Werne, J. P., Vanderwoude, A. J., Sinninghe Damsté, J. S., Hopmans, E. C., & Schouten, S. (2010). Applicability and calibration of the TEX_{86} paleothermometer in lakes. *Organic Geochemistry*, *41*(4), 404–413. https://doi.org/10.1016/j.orggeochem.2009.11.009

Prokopenko, A. A., Hinnov, L. A., Williams, D. F., & Kuzmin, M. I. (2006). Orbital forcing of continental climate during the Pleistocene: A complete astronomically tuned climatic record from Lake Baikal, SE Siberia. *Quaternary Science Reviews*, *25*(23–24), 3431–3457. https://doi.org/10.1016/j.quascirev.2006.10.002

Prokopenko, A. A., & Williams, D. F. (2004). Deglacial methane emission signals in the carbon isotopic record of Lake Baikal. *Earth and Planetary Science Letters*, *218*(1–2), 135–147. https://doi.org/10.1016/S0012-821X(03)00637-X

Qian, S., Yang, H., Dong, C., Wang, Y., Wu, J., Pei, H., et al. (2019). Rapid response of fossil tetraether lipids in lake sediments to seasonal environmental variables in a shallow lake in central China: Implications for the use of tetraether-based proxies. *Organic Geochemistry*, *128*, 108–121. https://doi.org/10.1016/j.orggeochem.2018.12.007

Raberg, J. H., Flores, E., Crump, S. E., de Wet, G., Dildar, N., Miller, G. H., et al. (2022). Intact Polar brGDGTs in Arctic Lake Catchments: Implications for Lipid Sources and Paleoclimate Applications. *Journal of Geophysical Research: Biogeosciences*, *127*(10). https://doi.org/10.1029/2022JG006969

Raberg, J. H., Harning, D. J., Crump, S. E., De Wet, G., Blumm, A., Kopf, S., et al. (2021). Revised fractional abundances and warm-season temperatures substantially improve brGDGT calibrations in lake sediments. *Biogeosciences*, *18*(12), 3579–3603. https://doi.org/10.5194/bg-18-3579-2021

Raberg, J. H., Miller, G. H., Geirsdóttir, Á., & Sepúlveda, J. (2022). Near-universal trends in brGDGT lipid distributions in nature. *Science Advances*, *8*(20), 1–13. https://doi.org/10.1126/sciadv.abm7625

Roberts, S. L., Swann, G. E. A., McGowan, S., Panizzo, V. N., Vologina, E. G., Sturm, M., & Mackay, A. W. (2018). Diatom evidence of 20th century ecosystem change in Lake Baikal, Siberia. *PLoS One*, *13*(12), e0208765. https://doi.org/10.1371/journal.pone.0208765

Russell, J. M., Hopmans, E. C., Loomis, S. E., Liang, J., & Sinninghe Damsté, J. S. (2018). Distributions of 5- and 6-methyl branched glycerol dialkyl glycerol tetraethers (brGDGTs) in East African lake sediment: Effects of temperature, pH, and new lacustrine paleotemperature calibrations. *Organic Geochemistry*, *117*, 56–69. https://doi.org/10.1016/j.orggeochem.2017.12.003

Shimaraev, M. N., Gnatovskii, R. Y., Blinov, V. V., & Zhdanov, A. A. (2006). Relationship between salinity and the ^{3}H-^{3}He age in deep water of Lake Baikal. *Doklady Earth Sciences*, *408*(4), 645–648. https://doi.org/10.1134/s1028334x06040301

Swann, G. E. A., Mackay, A. W., Vologina, E., Jones, M. D., Panizzo, V. N., Leng, M. J., et al. (2018). Lake Baikal isotope records of Holocene Central Asian precipitation. *Quaternary Science Reviews*, *189*, 210–222. https://doi.org/10.1016/j.quascirev.2018.04.013

Tarasov, P. E., Bezrukova, E., Karabanov, E., Nakagawa, T., Wagner, M., Kulagina, N., et al. (2007). Vegetation and climate dynamics during the Holocene and Eemian interglacials derived from Lake Baikal pollen records. *Palaeogeography, Palaeoclimatology, Palaeoecology*, *252*(3–4), 440–457. https://doi.org/10.1016/j.palaeo.2007.05.002

Tarasov, P. E., Bezrukova, E. V., & Krivonogov, S. K. (2009). Late Glacial and Holocene changes in vegetation cover and climate in southern Siberia derived from a 15 kyr long pollen record from Lake Kotokel. *Climate of the Past*, *5*(3), 285–295. https://doi.org/10.5194/cp-5-285-2009

Tarasov, P. E., Granoszewski, W., Bezrukova, E., Brewer, S., Nita, M., Abzaeva, A., & Oberhänsli, H. (2005). Quantitative reconstruction of the last interglacial vegetation and climate based on the pollen record from Lake Baikal, Russia. *Climate Dynamics*, *25*(6), 625–637. https://doi.org/10.1007/s00382-005-0045-0

Tierney, J. E., Poulsen, C. J., Montañez, I. P., Bhattacharya, T., Feng, R., Ford, H. L., et al. (2020). Past climates inform our future. *Science*, *370*(6517). https://doi.org/10.1126/science.aay3701

Toffolon, M., Piccolroaz, S., Majone, B., Soja, A., Peeters, F., Schmid, M., & Wüest, A. (2014). Prediction of surface temperature in lakes with different morphology using air temperature. *Limnology & Oceanography*, *59*(6), 2185–2202. https://doi.org/10.4319/lo.2014.59.6.2185

van Bree, L. G. J., Peterse, F., Baxter, A. J., De Crop, W., van Grinsven, S., Villanueva, L., et al. (2020). Seasonal variability and sources of in situ brGDGT production in a permanently stratified African crater lake. *Biogeosciences*, *17*(21), 5443–5463. https://doi.org/10.5194/bg-17-5443-2020

Wang, H., Chen, W., Zhao, H., Cao, Y., Hu, J., Zhao, Z., et al. (2023). Biomarker-based quantitative constraints on maximal soil-derived brGDGTs in modern lake sediments. *Earth and Planetary Science Letters*, *602*, 117947. https://doi.org/10.1016/j.epsl.2022.117947

Wang, H., Liu, W., He, Y., Zhou, A., Zhao, H., Liu, H., et al. (2021). Salinity-controlled isomerization of lacustrine brGDGTs impacts the associated MBT'_{5Me} terrestrial temperature index. *Geochimica et Cosmochimica Acta*, *305*, 33–48. https://doi.org/10.1016/j.gca.2021.05.004

Wang, H., Liu, W., & Lu, H. (2016). Appraisal of branched glycerol dialkyl glycerol tetraether-based indices for North China. *Organic Geochemistry*, *98*, 118–130. https://doi.org/10.1016/j.orggeochem.2016.05.013

Wang, H., Liu, Z., Zhao, H., Cao, Y., Hu, J., Lu, H., et al. (2024). New calibration of terrestrial brGDGT paleothermometer deconvolves distinct temperature responses of two isomer sets. *Earth and Planetary Science Letters*, *626*, 118497. https://doi.org/10.1016/j.epsl.2023.118497

Weber, Y., Sinninghe Damsté, J. S., Zopfi, J., De Jonge, C., Gilli, A., Schubert, C. J., et al. (2018). Redox-dependent niche differentiation provides evidence for multiple bacterial sources of glycerol tetraether lipids in lakes. *Proceedings of the National Academy of Sciences of the United States of America*, *115*(43), 10926–10931. https://doi.org/10.1073/pnas.1805186115

Weijers, J. W. H., Schouten, S., van den Donker, J. C., Hopmans, E. C., & Sinninghe Damsté, J. S. (2007). Environmental controls on bacterial tetraether membrane lipid distribution in soils. *Geochimica et Cosmochimica Acta*, *71*(3), 703–713. https://doi.org/10.1016/j.gca.2006.10.003

Weiss, R. F., Carmack Carmack, E. C., & Koropalov, V. M. (1991). Deep-water renewal and biological production in Lake Baikal. *Nature*, *349*(6311), 665–669. https://doi.org/10.1038/349665a0

Williams, D. F., Peck, J., Karabanov, E. B., Prokopenko, A. A., Kravchinsky, V., King, J., & Kuzmin, M. I. (1997). Lake Baikal record of continental climate response to orbital insolation during the past 5 million years. *Science*, *278*(5340), 1114–1117. https://doi.org/10.1126/science.278.5340.1114

Woolway, R. I., & Merchant, C. J. (2019). Worldwide alteration of lake mixing regimes in response to climate change. *Nature Geoscience*, *12*(4), 271–276. https://doi.org/10.1038/s41561-019-0322-x

Wu, J., Yang, H., Pancost, R. D., Naafs, B. D. A., Qian, S., Dang, X., et al. (2021). Variations in dissolved O_2 in a Chinese lake drive changes in microbial communities and impact sedimentary GDGT distributions. *Chemical Geology*, *579*, 120348. https://doi.org/10.1016/j.chemgeo.2021.120348

Xiao, W., Xu, Y., Ding, S., Wang, Y., Zhang, X., Yang, H., et al. (2015). Global calibration of a novel, branched GDGT-based soil pH proxy. *Organic Geochemistry*, *89–90*, 56–60. https://doi.org/10.1016/j.orggeochem.2015.10.005

Yang, H., Lü, X., Ding, W., Lei, Y., Dang, X., & Xie, S. (2015). The 6-methyl branched tetraethers significantly affect the performance of the methylation index (MBT') in soils from an altitudinal transect at Mount Shennongjia. *Organic Geochemistry*, *82*, 42–53. https://doi.org/10.1016/j.orggeochem.2015.02.003

Zhang, Y.-M., & Rock, C. O. (2008). Membrane lipid homeostasis in bacteria. *Nature Reviews Microbiology*, *6*(3), 222–233. https://doi.org/10.1038/nrmicro1839

Zhao, B., Castañeda, I. S., Bradley, R. S., Salacup, J. M., de Wet, G. A., Daniels, W. C., & Schneider, T. (2021). Development of an in situ branched GDGT calibration in Lake 578, southern Greenland. *Organic Geochemistry*, *152*, 104168. https://doi.org/10.1016/j.orggeochem.2020.104168

Zhao, B., Russell, J. M., Tsai, V. C., Blaus, A., Parish, M. C., Liang, J., et al. (2023). Evaluating global temperature calibrations for lacustrine branched GDGTs: Seasonal variability, paleoclimate implications, and future directions. *Quaternary Science Reviews*, *310*, 108124. https://doi.org/10.1016/j.quascirev.2023.108124

Zhu, Z., Wu, J., Rioual, P., Mingram, J., Yang, H., Zhang, B., et al. (2021). Evaluation of the sources and seasonal production of brGDGTs in lake Sihailongwan (N.E. China) and application to reconstruct paleo-temperatures over the period 60–8 ka BP. *Quaternary Science Reviews*, *261*, 106946. https://doi.org/10.1016/j.quascirev.2021.106946